TU Delft

Delft University of Technology

Document Version
Final published version

Licence
CC BY

Citation (APA)
Shah, S. S. M., Dewhurst, D. N., Giwelli, A., Raven, M. D., Ali, S. S. M., Geiger, S., & Busch, A. (2026). Core-scale evaluation of CO2 reinjection feasibility in a carbonate reservoir–caprock system: the S Field case study, Sarawak Basin, Malaysia. *Geoenergy*, *4*(1), Article 2025-046. https://doi.org/10.1144/geoenergy2025-046

Important note
To cite this publication, please use the final published version (if applicable).
Please check the document version above.

Copyright
In case the licence states “Dutch Copyright Act (Article 25fa)”, this publication was made available Green Open Access via the TU Delft Institutional Repository pursuant to Dutch Copyright Act (Article 25fa, the Taverne amendment). This provision does not affect copyright ownership.
Unless copyright is transferred by contract or statute, it remains with the copyright holder.

Sharing and reuse
Other than for strictly personal use, it is not permitted to download, forward or distribute the text or part of it, without the consent of the author(s) and/or copyright holder(s), unless the work is under an open content license such as Creative Commons.

Takedown policy
Please contact us and provide details if you believe this document breaches copyrights.
We will remove access to the work immediately and investigate your claim.

This work is downloaded from Delft University of Technology.

Research article

Geoenergy

https://doi.org/10.1144/geoenergy2025-046 | Vol. 4 | 2026 | geoenergy2025-046

Core-scale evaluation of CO_2 reinjection feasibility in a carbonate reservoir–caprock system: the S Field case study, Sarawak Basin, Malaysia

Sahriza Salwani Md Shah[1,2], David N. Dewhurst[3], Ausama Giwelli[3], Mark D. Raven[4], Siti Syareena M. Ali[2], Sebastian Geiger[5] and Andreas Busch[1]*

[1] Heriot-Watt University, Lyell Centre, Edinburgh, UK
[2] PETRONAS Research Sdn Bhd, Kuala Lumpur, Malaysia
[3] CSIRO Energy, Perth, Western Australia, Australia
[4] CSIRO Environment, Adelaide, South Australia, Australia
[5] Department of Geoscience and Engineering, Delft University of Technology, Delft, the Netherlands
DND, 0000-0001-9986-704X; AG, 0000-0002-5288-056X; MDR, 0000-0003-2635-9970; SSMA, 0009-0008-8166-7718; SG, 0000-0002-3792-1896; AB, 0000-0002-3279-5202
Present addresses: AG, Inpex, Perth, Western Australia, Australia
* Correspondence: a.busch@hw.ac.uk

Abstract: This study evaluates the feasibility of reinjecting separated CO_2 into its source carbonate reservoir, the high-temperature, high-pressure S Field in the Sarawak Basin, offshore Malaysia. The reservoir gas comprises ~30% CH_4 and ~70% CO_2. We combine mineralogical, petrophysical and geomechanical analyses to assess reservoir integrity and caprock sealing performance under *in situ* conditions. The calcite-dominated gas zone exhibits high porosity (>30%), whereas the underlying aquifer zone is co-dominated by calcite and dolomite with lower porosity (20–25%) and higher strength. The primary caprock (Seal A), a 500 m-thick Miocene mudrock–siltstone unit, has porosities of 2–10% and low permeability, with illite and quartz as dominant minerals. Laboratory experiments exposed reservoir and caprock samples to CO_2-charged brines at reservoir pressure (30 MPa) and temperature (150°C) for up to six months. Post-reaction analyses revealed only minor changes in mineralogy, porosity, permeability and mechanical strength. These results indicate limited CO_2–water–rock reactivity and confirm the mechanical and geochemical stability of both reservoir and caprock. The findings support the viability of CO_2 reinjection and long-term geological storage in the S Field, providing a benchmark case for carbonate-hosted carbon capture and storage systems in SE Asia.

Supplementary material: Petrophysical, mineralogical, geochemical data are available at https://doi.org/10.6084/m9.figshare.c.8459525

Thematic collection: This article is part of the CCS in the Asia–Pacific region collection available at: https://www.lyellcollection.org/topic/collections/ccs-asia-pacific

Received 20 October 2025; **revised** 19 January 2026; **accepted** 24 March 2026

Abundant natural gas reservoirs have been detected in Miocene carbonate build-ups in the offshore Sarawak Basin, Malaysia (Darman and Harun 2006). However, this cluster of gas fields contains high contents of CO_2 (>40%) which are challenging for field development. Therefore, carbon capture and storage (CCS) has been identified as one of the solutions to manage the high CO_2 levels and to monetize and sustain the gas production. Integrated screening and site selection for potential CO_2 storage sites for these high CO_2 fields have been conducted previously (Bing *et al.* 2015; Widyanita 2017). These feasibility studies involve the implementation of cyclic gas production and CO_2 reinjection from the start of the field operation. The CO_2 reinjection into the same or an overlying/underlying reservoir provides the advantage of no transportation costs, a concept that has already been applied successfully within the Norwegian Sleipner Field (IPCC 2009). However, there are limited case studies of CO_2 storage in carbonate reservoirs compared to clastic reservoirs and most of these CCS projects are related to enhanced oil recovery (EOR) operations, such as in the Weyburn Field in Canada, the West Seminole San Andres Unit in Texas, USA or the Lula Field in Brazil (Brown *et al.* 2017; Siqueira *et al.* 2017; McCloskey *et al.* 2022).

The viability of CO_2 storage in the S Field hinges on two critical factors: (i) the geochemical reactivity of the carbonate reservoir rock and (ii) the sealing capacity and mechanical stability of the overlying caprock formations (Seal A and Seal B). Carbonate minerals, such as calcite and dolomite, are known to dissolve in low-pH environments, potentially altering porosity, permeability and mechanical strength. Additionally, the interaction of supercritical CO_2 with fine-grained mudrocks may affect the mineralogy and induce microstructural changes that compromise seal integrity.

Previous geochemical modelling of the S Field (Ameer Hamza *et al.* 2012) suggested limited mineralogical changes upon CO_2 exposure; however, these predictions were based on limited input data and lacked experimental validation. To date, there has been no systematic study incorporating integrated mineralogical, petrophysical and geomechanical analyses under simulated reservoir conditions. This study addresses these knowledge gaps through detailed laboratory investigations designed to replicate *in situ* CO_2–water–rock interactions. The objective is to assess the suitability of the S Field for safe, long-term geological CO_2 storage and to contribute to the broader understanding of CCS feasibility in carbonate-dominated systems.

© 2026 The Author(s). This is an Open Access article distributed under the terms of the Creative Commons Attribution License (http://creativecommons.org/licenses/by/4.0/). Published by The Geological Society of London for GSL and EAGE. Publishing disclaimer: https://www.lyellcollection.org/publishing-hub/publishing-ethics

Downloaded from http://pubs.geoscienceworld.org/gsl/geoenergy/article-pdf/doi/10.1144/geoenergy2025-046/7859514/geoenergy2025-046.pdf by TU DelftLibrary user on 10 J

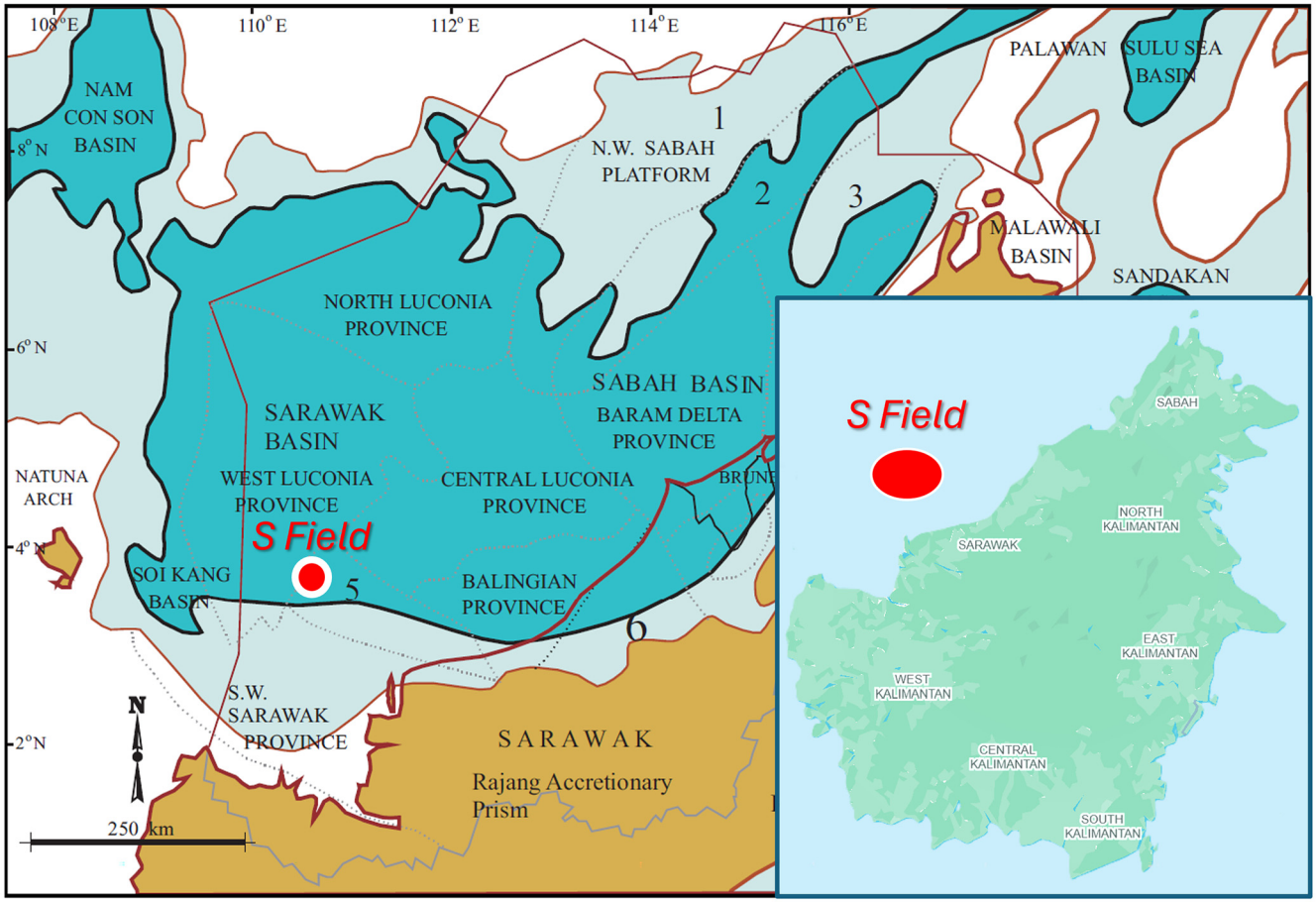


Fig. 1. Map showing the hydrocarbon provinces of the Sarawak and NW Sabah basins as well as the location of the S Field in the Tatau Province, in the south of the Sarawak Basin. (1) NW Sabah Platform, (2) NW Sabah Trough, (3) Outboard Belt, (5) Tatau Province, (6) Tinjar Province. Source: modified after Tjia (2012).

Geological setting

The Sarawak Basin

The S Field is located 200 km offshore Sarawak in the Tatau Province in the Sarawak Basin, East Malaysia (Fig. 1). This Cenozoic sedimentary basin developed by straddling collisional plate boundaries as part of the regional development of SE Asia, which lies at the junction between the Eurasian Indo-Australian, Pacific and Philippine Sea plates (Tjia 2000; Metcalfe 2009, 2011). From a seismic stratigraphy study, it was concluded that the Sarawak Basin formed by NW–SE-trending right-lateral movement during the late Oligocene–Miocene (Zin 1997). The continental margin of the Sarawak Basin forms part of the Late Eocene of the Sundaland landmass (Madon 1999). The Nam Con Basin bounds the Sarawak Basin to the NW, the Sabah Basin to the east and the Soi Kang Basin to the SW (Fig. 1). The Sarawak Basin extends ~400 km in a north–south direction and ~740 km east–west (Tjia 2012).

Sedimentation in the Sarawak Basin was mainly in coastal to shallow marine environments during the Oligocene and Early Miocene. During the Middle Miocene, tectonic activity resulted in extensional faulting and the creation of depocentres and intervening basement highs. A relative rise in sea-level during this event resulted in marine conditions offshore Sarawak and the deposition of shallow carbonates on partly submerged basement highs (Madon and Redzuan 1999). Eight phases, called 'Cycles', have been used to describe the sedimentation from the Late Eocene to the Pleistocene in the Sarawak Basin (Lunt and Madon 2017). These Cycles were defined by an initial transgression, changing gradually to regression and tied with planktonic foraminifera (Ho 1978). The contrast in lithology marked the boundary of each cycle. Sea-level transgressions spread over a wide area; thus the sediment characteristic and depositional environment can be different even within the same cycle (Lunt and Madon 2017). For example, in the Baram Province, Cycles I and II formed deep marine sediments, in contrast with the coastal and fluviomarine sediments in the Balingian Province (Fig. 1). Cycle III generally characterizes deltaic environments and defines the base of carbonate build-ups in Cycle IV. Cycles IV and V sediments are both carbonate build-ups. The Sarawak Basin is subdivided into five provinces which represent an area characterized by a particular tectonic and structural style that influenced the stratigraphic and sedimentation histories. The provinces are Baram Delta, Balingian, Luconia (West, North and Central), Tinjar and Tatau (Tjia 2012), with the S Field being located in the latter province (Fig. 1). Horst and graben structures make up the Tatau region. Situated between the Balingian and SW Sarawak provinces, the Tatau Province is divided into the Half-Graben and SW Luconia sub-provinces, separated by the Penian High (Fig. 1).

Middle Miocene extensional tectonics overprint the structure of the Tatau Province by creating NNW-trending normal faults, dipping mostly to the SW (Madon and Redzuan 1999; Sim and Jaegar 2006). Fault movement during Cycles III and IV resulted in the development of deep half-graben, filled with thick Cycle III to V sediments. At the end of Cycle III, the area underwent compressional deformation, followed by the development of carbonate build-ups on the uplifted horsts (Madon and Redzuan 1999).

Downloaded from http://pubs.geoscienceworld.org/gsl/geoenergy/article-pdf/doi/10.1144/geoenergy2025-046/7859514/geoenergy2025-046.pdf by TU DelftLibrary user on 10 J

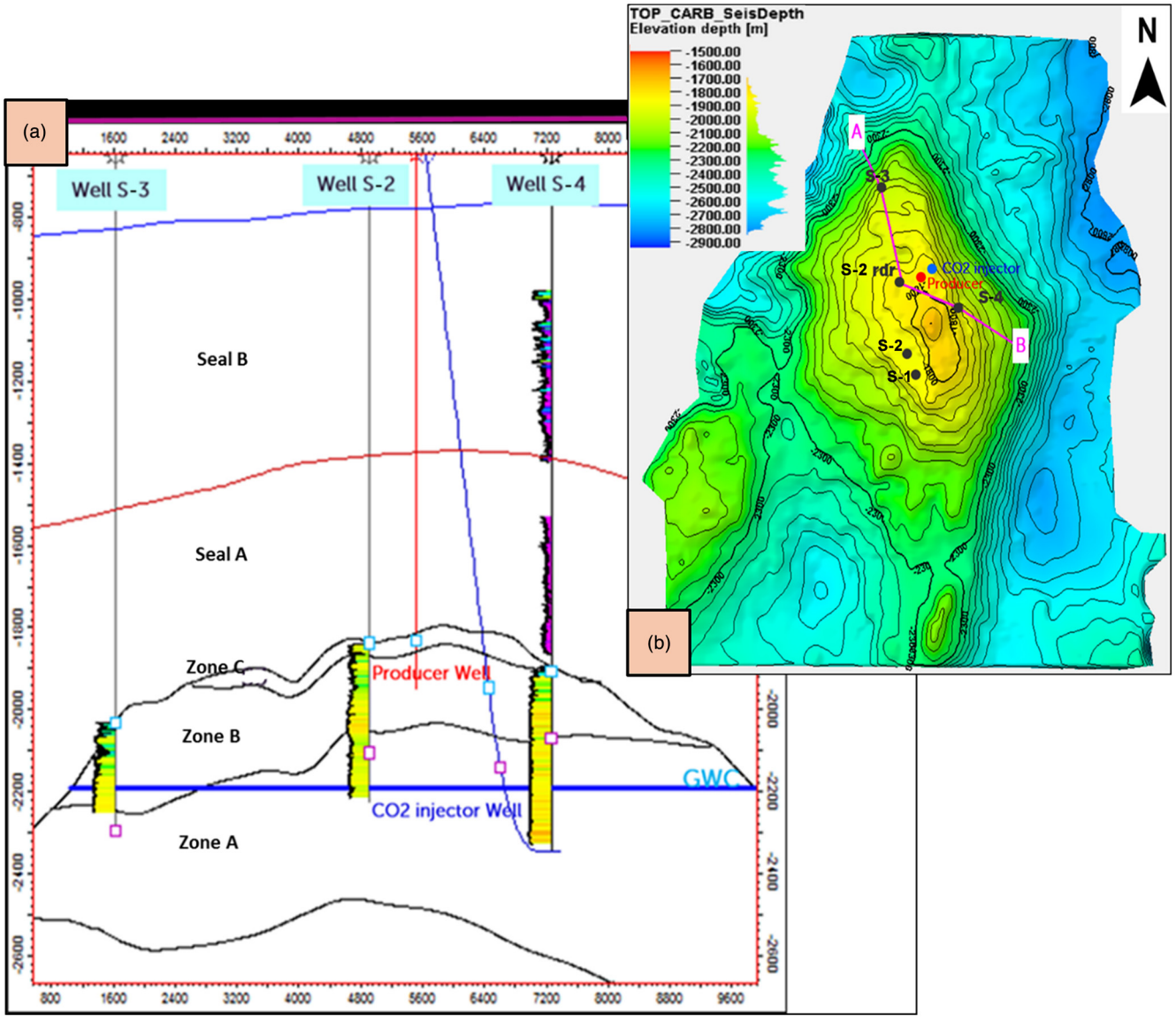


Fig. 2. (**a**) Cross-section of wells S-3 to S-4 showing the depth penetration of the wells drilled into the S Field in metres and (**b**) proposed well location for CO_2 injection into the aquifer zone below the gas/water contact. Horizontal scale in metres. Inset map shows the line of cross-section over the S Field and the four-way closure of the structure.

Overview of the S Field

Reservoir setting

Palaeoenvironmental studies indicate that the Tatau Province formed in a non-marine setting in Cycles I to IV (Oligocene to Middle Miocene; Madon and Redzuan 1999). Carbonate build-ups start to develop during the regional marine transgression in Cycle IV. Cycle V and younger are believed to be deposited in deltaic and shallow marine environments. Particularly for the S Field, the palaeoenvironment evolves from lower coastal plains in Cycle I to coastal plains in Cycles II and III, and finally to a neritic environment with the start of the carbonate build-ups in Cycles IV and V (Madon and Redzuan 1999).

The S Field structure (Fig. 2) is a north–south elongated four-way dip closure carbonate build-up with a vertical relief of more than 300 m. The build-up covers an area of ~102 km^2. The water depth for this area is approximately 80 m. The most recent well, S-4, was drilled in 2015, after S-1 (1970), S-2 (1997), S-2 rdr (1997) and S-3 (2006). The first core from Cycles IV and V carbonate build-ups was obtained from the S-3 well, providing 44 m of carbonate material. Well S-4 provides access to 200 m of carbonate core and 18 m of overlying caprock material. The caprock material has been cored just above the reservoir section and is expected to be representative for initial reaction/leakage should this occur. Core samples and drill cuttings from all wells were used in this study to identify the overall distribution of mineralogy as well as interpretation of the depositional environment for the S Field.

Three connected reservoir zones (Zones A, B and C) are determined based on stratigraphy, formation pressure and petrophysical log interpretation and analysis (Fig. 2). The top of the carbonate, referred to as Zone C, has a thickness of up to 150 m at the crest and thins out towards the flanks with a thickness of ~30 m. The second carbonate zone (Zone B) is further divided into two zones with different reservoir quality. The upper part of Zone B is the main production/hydrocarbon zone with good porosity and permeability. The deeper carbonate zone at depths below ~2000 m (Zone A) forms the gas and aquifer zone. Gas/water contact is estimated at 2193 m across the reservoir (Fig. 2). The top of the carbonate reservoir is overlain by two sealing units, comprising the caprock. The effective seal, and one of the focus areas of this study, is Seal A with a thickness of ~300 m at the crest and up to 500 m towards the flanks of the top of the carbonate. The second layer (secondary seal) is Seal B with a thickness of ~800 m (Fig. 2).

Downloaded from http://pubs.geoscienceworld.org/gsl/geoenergy/article-pdf/doi/10.1144/geoenergy2025-046/7859514/geoenergy2025-046.pdf by TU DelftLibrary user on 10 J

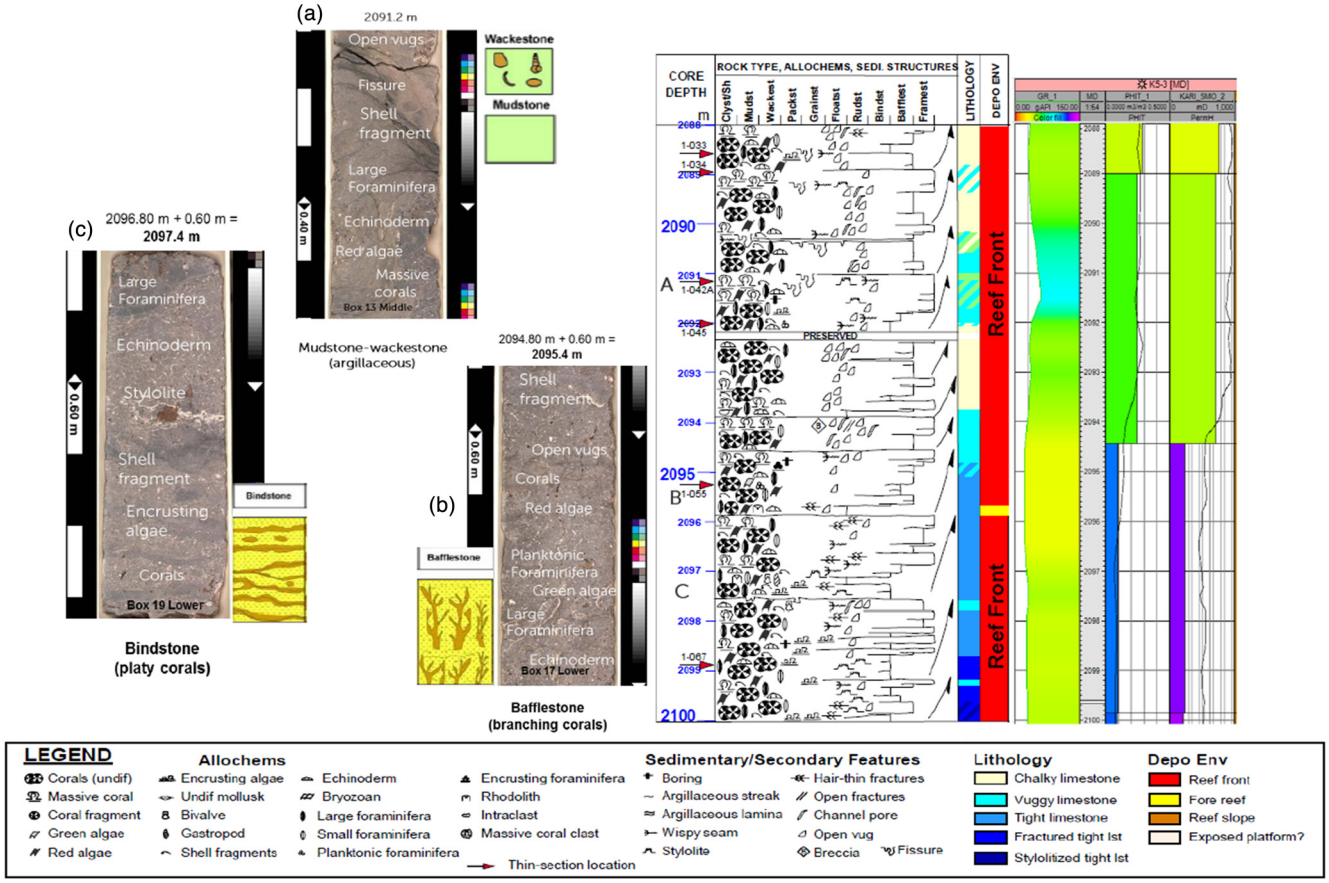


Fig. 3. Core description and facies association of core at a depth of 2088–2100 m from the S-3 well. The depositional environment is interpreted to be a reef front setting with lithofacies association dominated by bafflestone, bindstone and framestone. These three lithofacies are composed of large grain/allochem components that are bound together during deposition, indicating a high energy environment. The short core section A shows lamination of shale in the mudstone–wackestone lithofacies. Core section B portrays branching corals with red and green algae in between the coral fragments. Platy corals shown in the core section C, together with sedimentary structure of stylolite, may indicate lamination of shale in the mudstone–wackestone lithofacies. Core section B portrays the branching coral with red and green algae in between the coral fragments. Platy corals are shown in core section C, together with sedimentary structures associated with stylolites.

The high CO_2 contents of the S Field (~70%) are assumed to originate from thermal breakdown of organic matter or from inorganic sources such as mantle degassing (Cooper *et al.* 1997). Stable isotope data from reservoir fluids provide evidence of a thermogenic origin of the gases (Madon and Redzuan 1999). The $\delta^{13}C$ isotopic composition in the S Field ranges from −38 to −33‰, suggesting a post-mature generation stage; thus, the high CO_2 content in the S Field can be related to migration of CO_2 from deeply buried sources (at high temperature) along extensional normal faults (Madon and Redzuan 1999).

Depositional environment of the S Field

The first biostratigraphy studies on samples from well S-1 indicated deposition of the carbonate reservoir and Seal A in the Middle Miocene (11–16 Ma), whereas Seal B was deposited in the Late Miocene (~5–10 Ma). Foraminifera *Globorotalia mayeri* was discovered in the carbonate reservoir and marks a Middle Miocene age (12 Ma), while *Globorotalia margaritae* found in the overlying mudrock samples (Seal B) indicates a Late Miocene/Early Pliocene (5–7 Ma) deposition (Bolli and Saunders 1982; Liska 1991; Rehm 2003; Wade *et al.* 2018).

The depositional environment of the S Field is associated with lagoonal to back reef and off reef facies, with seven main lithofacies described from the sampled intervals. The lithofacies were characterized by combining the classifications of Dunham (1962) and Embry and Klovan (1971), described in (Flügel 2004). This classification is based on depositional texture and origin, including grain composition and grain size, as well as biogenic content and sedimentary structures.

This study analyses carbonate reservoir variability and identifies eight lithofacies in the carbonate core samples of the S Field, namely wackestone, bafflestone, packstone, grainstone, floatstone, rudstone, bindstone and framestone. The S Field carbonate records repeated phases of shallowing and deepening as evidenced from palaeobathymetric data and facies associations (Fig. 3). The carbonate core section, derived from the S-3 well, is dominated by large grain lithofacies, which suggests the depositional environment as reef front.

The heterogeneity of lithofacies influences the mineralogy and rock quality, shown in core samples from well S-4 (Fig. 4). Representative samples for each dominant lithofacies in the S Field show variable porosity, permeability, pore type and mineralogy. Rudstone is the dominant lithofacies in the S-4 well. Porosity and permeability determined on rudstone show the highest values compared with other samples, which is due to high porosity associated with mouldic and vuggy pores. Floatstone and bindstone show low porosity and permeability, reflecting highly cemented carbonate rocks as part of this lithofacies. The differences of rock quality and mineralogy for these lithotypes plays an important role in the reservoir heterogeneity of the S Field.

S Field as a CO_2 storage reservoir

CCS implementation was planned to start with the production of natural gas (~70% CO_2, ~30% CH_4), followed by CO_2 separation and

Downloaded from http://pubs.geoscienceworld.org/gsl/geoenergy/article-pdf/doi/10.1144/geoenergy2025-046/7859514/geoenergy2025-046.pdf by TU DelftLibrary user on 10

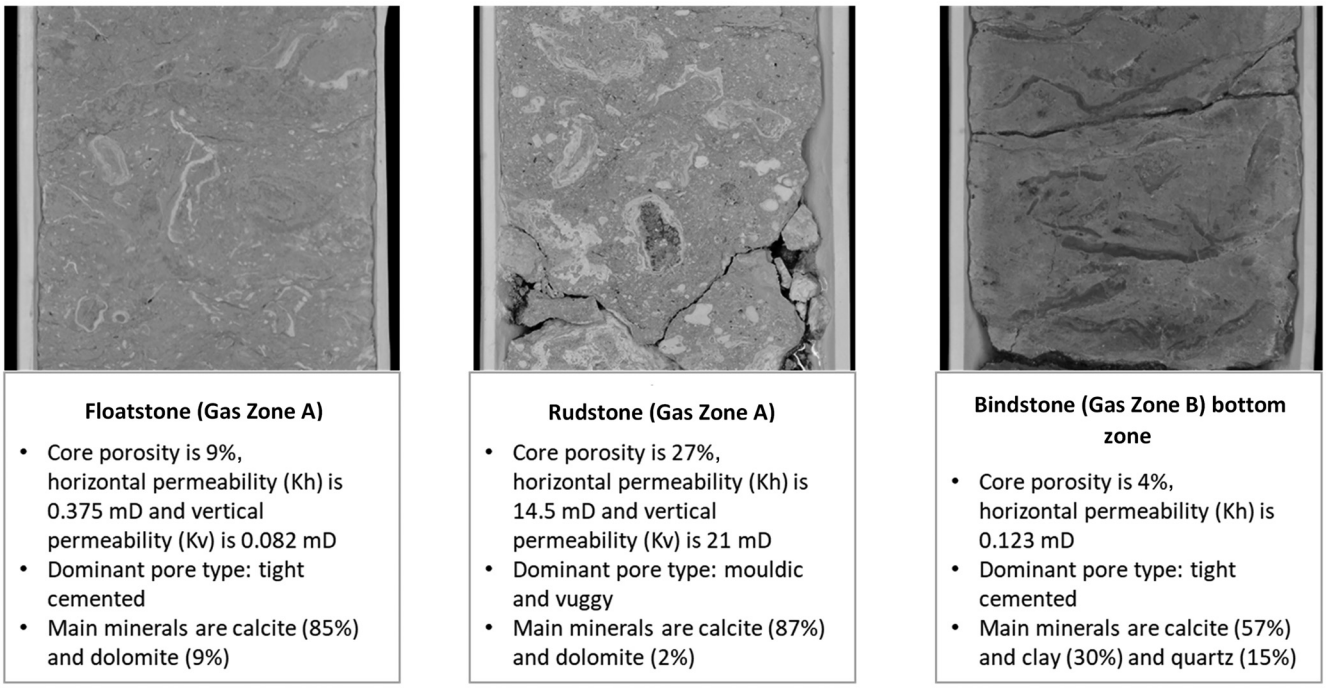


Fig. 4. Core photographs from well S-4 show the differences in core porosity and permeability for different lithofacies. These three lithofacies are the main lithofacies in the gas zone formation. Rudstone represents the most dominant lithofacies with high porosity and permeability and this can be related to the mouldic and vuggy pore type. The pores in the floatstone are cemented, resulting in low porosity and permeability. Bindstone from the bottom Zone B has the lowest porosity and permeability and this can be related to the presence of clay minerals, which fill pores in between the allochem during the carbonate exposure.

reinjection into the aquifer zone (Fig. 2). This concept will change the current pressure, temperature, mechanical and geochemical equilibria of the S Field. The initial formation pressure of the S Field is ~35 MPa and the temperature is ~150°C at a depth of ~2200 m, resulting in a CO_2 partial pressure of 24.5 MPa. The high concentration of CO_2 in the gas zone indicates that exsolution happened, as the formation brine is almost fully saturated with CO_2 (Zaidin *et al.* 2019). As a result, the reservoir pressure will decrease during gas production, which may also reduce the CO_2 solubility into formation water, and trigger CO_2 exsolution from the water into the gas zone (Kuo 1997). However, following CO_2 reinjection, the reservoir pressure will slightly recover, together with the CO_2 partial pressure. Ultimately, this will result in re-equilibration of pore fluids with CO_2.

CO_2 infill into the reservoir resulted in a (near) equilibrium state between rocks and CO_2-charged fluids (Kaszuba *et al.* 2011; Bickle *et al.* 2013). Consequently, the increase of the CO_2 partial pressure is expected to result in minimal changes in pH/alkalinity and therefore in small-scale mineral reactions with the injected CO_2 only. However, this scenario requires validation by an integrated analytical and numerical study to establish an appropriate subsurface risk assessment.

Samples, data and methods

We used a combined petrophysical, mineralogical, geochemical and geomechanical approach to characterize the caprock (Seal A and Seal B) and carbonate reservoir properties of S Field. This approach is complemented by integrating field data, such as formation fluid compositions (gas and brine), formation stress, temperature, pressure, petrophysical well log analysis and well/field testing of the S Field. Reservoir pressure, temperature and *in situ* stress were used in laboratory studies to simulate the actual reservoir conditions. Wireline data, which has mainly been used as background data and to inform some of the interpretation of this study, can be found in the Supplementary material (SI 1).

Reservoir condition and reservoir fluid properties

Reservoir pressure and temperature

Data recorded from the five wells show formation pore pressures of 33.8–35.2 MPa for the gas zone (1925–2195 m depth) and up to 36.5 MPa in the aquifer zone at a depth of 2300 m, indicating significant over-pressurization of the formations of ~15 MPa. The temperature gradient is based on formation test data and each well provides different temperature gradients, depending on the well location in the reservoir structure. For the S-4 well, within the carbonate reservoir, the temperature ranges from 108°C at depth 1925 m (~5.6°C per 100 m); for the S-2 rdr well, the true vertical depth subsea to 130°C is at datum 2193 m (~5.9°C per 100 m), indicating a high temperature anomaly in the CO_2 storage target formation.

Reservoir fluid compositions

Only the S-3 and S-4 wells provide information on brine composition, although data from both wells differ. The brine salinity in well S-3 is 40 000 ppm, but it is considered to be contaminated and not representative as it is a surface sample. The brine salinity in well S-4 is considered low (9000 ppm) in comparison to other salinities recorded in the Sarawak Basin, such as in the Jintan Field, which yields a salinity of about 20 000 ppm. Thus, the synthetic brine is based on the relative brine composition obtained from S-4 well but with a salinity of ~20 000 ppm to be comparable to regional salinities recorded in the Sarawak Basin/average salinity in neighbouring fields (PETRONAS, unpublished data). This salinity has been used in all laboratory experiments (Table 1).

The reservoir gas composition in the S Field is determined by analysis of the mud gas as well as from formation testing and gas sampling. The ratio of methane (C1) to n-heptane (nC5) increases with depth. Formation tests in all wells provide average CO_2

Downloaded from http://pubs.geoscienceworld.org/gsl/geoenergy/article-pdf/doi/10.1144/geoenergy2025-046/7859514/geoenergy2025-046.pdf by TU DelftLibrary user on 10 J

Table 1. Brine composition used for laboratory analysis (in ppm)

Ca^{2+}	Mg^{2+}	K^{+}	Na^{+}	Sr^{2+}	HCO^{3-}	Cl^{-}	SO_4^{2-}	TDS
247	46	311	7653	73	400	12 348	182	21 056

TDS, total dissolved solids.

contents ranging between 63% and 90%, and 30–290 ppm for H_2S in the gas zones. All tests were conducted in the gas zones, except Test 1 in the S-4 well, which was conducted in the aquifer zone. The tests further indicate significantly higher CO_2 concentrations in the aquifer zone, reaching values of close to 100%, with 500 ppm of H_2S. The higher concentration of CO_2 in the water zone is similar to the measured CO_2 composition obtained from PVT analysis, showing an average of 70 mol% CO_2 in the gas zone and 100 mol% of CO_2 in the aquifer zone.

Samples and sample preparation

About 700 carbonate and shale core plugs were obtained from well S-4 for determining petrophysical and mechanical properties. In addition, a selection of the core chips and drill cuttings was collected for mineralogical analysis. Full diameter whole-core medical CT scanning was performed at 0 and 90° longitudinal orientations along the core. CT scan images were used to evaluate the internal core condition and quality before deciding on exact sampling and plugging locations. This is an important workflow process, especially for selecting samples for geomechanical testing, which requires intact and identical samples for triaxial testing under different stress conditions.

Carbonate samples were slabbed and then plugged two-thirds across the longitudinal section. The carbonate core was cleaned using toluene and methanol by cold Soxhlet extraction. After extraction, the plugs were dried using two methods: (1) humidity oven at 60°C and 45% relative humidity for rock mechanical experiments and (2) 60°C for routine core analysis.

Shale sample preservation is more critical as loss of initial pore fluids can change initial properties, such as the hydration state of swelling clay minerals, ultimately leading to dehydration cracking or fracturing due to general stress-unloading (Ewy 2015). In addition, shales can become stronger and stiffer on the loss of native pore fluids (e.g. Pervukhina *et al.* 2015; Minaeian *et al.* 2017). Therefore, shale whole-core sections were kept in non-polar mineral oil and were not slabbed before plugging using a diamond wire band saw (details in Dewhurst *et al.* 2020). This is the recommended method to avoid dehydration of the samples (Ewy 2018).

Experimental methods

In this study, we aim for a multi-method, comprehensive characterization of the reservoir as well as analysing the effects of CO_2–water–rock interactions (CO_2WRI) on these reservoir properties. Reservoir characterization involves fluid geochemistry and mineralogy, as well as routine and advanced petrophysical/geomechanical core analysis. CO_2WRI involve batch experiments, together with pre- and post-geomechanical, mineralogical and petrophysical analysis, for which core samples from both reservoir and caprocks have been used. Table 2 provides details of methods used and the number of samples tested in this study.

Reservoir and caprock characterization

Detailed descriptions of the standard experimental methods (helium porosity, air permeability on carbonates, X-ray diffraction (XRD) and X-ray fluorescence (XRF) analysis, scanning electron microscopy, mercury injection capillary pressure) and details for the CO_2 ageing experiments are summarized in the Supplementary material (SI 2). Methods requiring specific explanations are detailed below.

We used the unsteady-state pulse decay method (Brace *et al.* 1968) to measure permeability on shale samples from Seal A. Analytical and numerical methods have been established to determine the intrinsic permeability and porosity from one single experiment (Cui *et al.* 2009; Profice *et al.* 2012). The method considers unconfined samples that are charged with a helium gas pressure. Permeability is then calculated from the pressure decay

Table 2. List of work scopes with detail of testing conditions and location

Work scope	Samples and testing conditions
Core review and description	200 m reservoir and 18 m caprock from S-4 well
Mineralogy and petrography	
X-ray diffraction (XRD)	Reservoir (40); caprock (40)
Scanning electron microscopy (SEM)	Reservoir (10)
Thin section analysis	Reservoir (13)
Specific surface area (SSA)	Reservoir (11); caprock (1)
Cation exchange capacity (CEC)	Reservoir (5); caprock (5)
X-ray fluorescence (XRF) analysis	Reservoir (5); caprock (5)
Petrophysics	
Permeability	Seal A (1); reservoir (682)
Mercury injection capillary pressure	Seal A (5)
Porosity	Reservoir (682)
CO_2–water–rock Interactions (CO_2WRI)	
Rock chip reaction tests	1 sample from each reservoir zone (A, B, C) and seal (A, B)
Core plugs reaction tests	10 samples from each water zone, gas zone A and gas zone B
Petrophysical and rock mechanical testing	60 samples: 3 samples each from water zone, gas zones A and B for pre- and post-CO_2WRI using triaxial and Brazilian testing; 30 samples for porosity and permeability measurement after CO_2WRI
Batch experiment to study changes in rock strength	14 core plugs from Seal A
Rock mechanical tests for pre- and post-CO_2WRI	12 samples from Seal A

Numbers in brackets indicate number of samples.

Downloaded from http://pubs.geoscienceworld.org/gsl/geoenergy/article-pdf/doi/10.1144/geoenergy2025-046/7859514/geoenergy2025-046.pdf by TU DelftLibrary user on 10 J

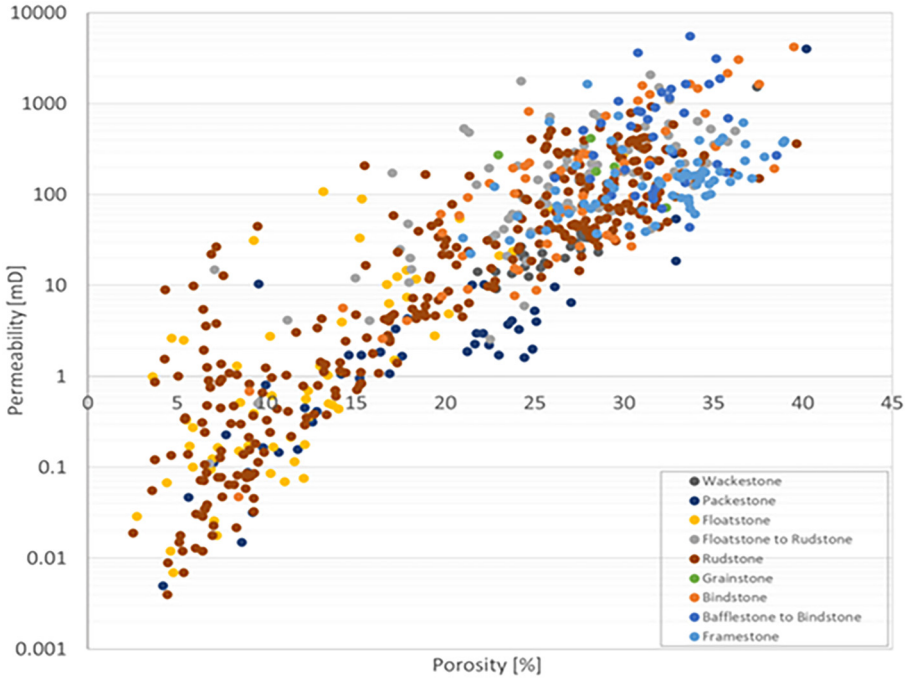


Fig. 5. Lithofacies distribution plotted with porosity and permeability. Lithofacies with large sizes of grain/allochems, such as framestone, bafflestone, bindstone and grainstone, dominate the high porosity and permeability values.

curve and porosity at pressure equilibrium. We used one core plug sample from well S-4 with dimensions of 25.4 mm in diameter and 19.6 mm in length, which was oven-dried at 105°C under vacuum. The measurement was repeated three times, resulting in average permeability values of 0.47 μD (4.7×10^{-19} m^2). It should be noted that drying the sample may have impacted the results, allowing cracks to form. Actual water permeability may therefore be significantly lower.

In total, 30 core plug samples from the carbonate reservoir and 12 samples from Seal A caprock were used for triaxial testing and Brazilian indirect tensile strength testing. Cylindrical samples were cored normal to bedding for triaxial tests, with dimensions of 38 mm in diameter and 76 mm in length for carbonate, and 25 mm in diameter and 50 mm in length for shale caprock. Single-stage triaxial testing was conducted on sets of three samples for each depth using a Terratek triaxial testing machine and an autonomous triaxial cell developed by CSIRO (Dewhurst and Siggins 2006; Dewhurst *et al.* 2011; Kuila *et al.* 2011).

The operational limits of the rigs are 70 MPa confining pressure (with oil used as a confining medium), 70 MPa pore pressure and 400 kN axial load. All experiments were conducted at room temperature of 22 ± 0.5°C and no diurnal pore pressure fluctuations were noted. Each sample was tested with different confining stresses within the range of the *in situ* minimum horizontal stress. Confining pressures range between 36 and 66 MPa for the shale samples, 40.5 and 60.5 MPa for samples from gas zone A, 39 and 50 MPa for gas zone B, and 40 and 55 MPa for the aquifer zone samples. Another set of samples from each zone was tested using different confining pressures following CO_2 ageing. Shale samples from Seal A were dry after CO_2 ageing, so no pore pressure was applied. The range of confining pressure used during testing of the aged samples from Seal A was 6–25 MPa and the values were matched to the effective stress conditions in the saturated shale samples. Details of the tests on the seal samples have been published previously (Dewhurst *et al.* 2020) so will be only briefly summarized here. During testing for aged reservoir samples, the confining pressures were similar to those without ageing for gas zone A samples. The ranges were 40.5–50.4 MPa, 39–55 MPa for aged samples from gas zone B and 40–55 MPa for aquifer zone samples. The pore pressure applied to the samples was determined from the *in situ* pore pressure, using 30 MPa for shale samples, ~34.7 MPa for samples from gas zone B, 35.2 MPa for gas zone A and 36.7 MPa for aquifer zone samples. Carbonate samples were isotropically consolidated in a drained state before axial loading at a strain rate of 1.0×10^{-6} s^{-1}. A different setup was used for shale as the axial load was applied under undrained conditions (pore pressure lines closed) at a lower strain rate of 1.0×10^{-7} s^{-1} until failure occurred. Shale samples were left for consolidation for two to three weeks before undrained axial loading was applied to the sample tested. Stress, strain and pore pressure were monitored during loading/deformation. Stress–strain curves from this triaxial testing provided information on elastic–plastic behaviour and derivation of elastic moduli such as Young's modulus and Poisson's ratio as well as yield strength. Principal stresses from each sample for individual depths were plotted on Mohr's circles to determine the failure envelope and compressive strength.

Brazilian testing was performed on six carbonate and two preserved shale samples to evaluate the indirect tensile strength (Riding and Rochelle 2009; Perras and Diederichs 2014). Disc-shaped plugs with nominal dimensions of 38 mm in diameter and 20 mm in length were loaded into standard Brazilian jaw platens with transducers connected to measure the axial deformation (mm) and axial load (kN). The samples were loaded at 0.01 mm min^{-1} until failure. The tensile stress along the diameter was calculated according to ASTM (2008) and ISRM (1978).

Results and discussion

Initial characterization of reservoir and caprock in S Field

Porosity and permeability of carbonates

Porosity and permeability were measured on 682 carbonate plugs from well S-4. The results reveal a wide range of heterogeneity (Fig. 5), attributed to variations in lithofacies, depositional environment and diagenetic sequence (Masoudi *et al.* 2011; Wilson *et al.* 2013; Janjuhah and Alansari 2019; Warrlich *et al.* 2019; Ali *et al.* 2021). Laboratory data indicate that around 30% of the samples are highly porous carbonates, exhibiting porosities >30% and permeabilities >100 mD. Four dominant pore types are identified during core plug description: mouldic and vuggy (PT1)

Downloaded from http://pubs.geoscienceworld.org/gsl/geoenergy/article-pdf/doi/10.1144/geoenergy2025-046/7859514/geoenergy2025-046.pdf by TU DelftLibrary user on 10 J

are the main pore types, averaging 48% of the total core plugs, followed by intergranular pore types (PT2) with 28%; 18% relate to cemented pore types (PT3); and 6% of the core plugs are characterized by fractures (PT4). All pore types are found in the gas zone but only two pore types in the aquifer zone (intergranular and cemented). The differences reflect that porosity along well S-4 varies, particularly comparing rock quality in the gas and the aquifer zones. Porosity in the gas zone ranges from 2 to 40%, while the aquifer zone is between 7 and 28%. Consequently, the three different layers of the gas zone have higher permeabilities of up to 5000 mD, compared to the aquifer zone with maximum values of 33 mD. However, samples from the top of the carbonate have low porosities, mainly characterized by cemented and intergranular pore types.

Mouldic and vuggy pore types dominate the higher range and cemented pore types dominate the lower range of porosity and permeability (Fig. 5). Samples identified with fractured and intergranular pore types are found to be scattered across the plot from low to high porosity and permeability ranges.

The porosity types observed are classified as secondary porosity based on the diagenetic features observed in the core samples. The evolution of secondary porosity from primary porosity is interpreted to be due to dolomitization and dissolution or leaching of skeletal allochems (Moore 1989; Zampetti *et al.* 2003; Wayne 2008). The dominant pore types identified in the S Field carbonates are similar to adjacent carbonate gas fields in the Central Luconia Province of the central Sarawak Basin (Pierson *et al.* 2012; Janjuhah *et al.* 2017*a*; Janjuhah and Alansari 2019; Ali *et al.* 2021).

In relation to lithofacies, the measured porosity and permeability values match quite well the textural classification scheme by Dunham (1962), modified by Embry and Klovan (1971). Core plugs with lithofacies made up of large grain/allochem sizes (>30 mm), such as framestone, bindstone and bafflestone, are found to have high porosities and permeabilities (Fig. 5). The rudstone lithofacies has a scattered distribution across the plot from low to high values, which is expected as the grain/allochem size in this rock type is highly variable.

Detailed analysis reveals that the core plug samples dominated by mouldic and vuggy pore types (PT1) are grain-supported carbonates such as framestone and bindstone. Samples that are dominated by intergranular (PT2, PT3) pore types are mostly mud-supported carbonates such as packstone and wackestone. This comparison reflects the influence of diagenesis and matrix composition on carbonate rock quality and pore connectivity.

Similar observations were made in the petrographic study, which was conducted on ten carbonate core samples from well S-4. The objective was to obtain a detailed description of the texture, composition and diagenesis of the samples. From a microscopic scale, three main pore types were identified, which are intergranular, intragranular, as well as vuggy/mouldic. The primary porosity (intergranular and intragranular pores) is associated with the original depositional texture (Flügel 2004; Wayne 2008).

From microscopic analysis, the allochems appear to be poorly preserved, with most of them experiencing neomorphism. This diagenetic process leads to the formation of micritic and sparry calcite in between the remaining allochems. As a result, the grains/allochems are poorly to moderately sorted. Only few types of bioclasts can still be identified, including remnants of corals, algae, benthic foraminifera, echinoderms, bryozoans and bivalves. From the grain sorting and texture, three lithotypes were identified using Dunham's classification: (1) wackestone–packstone; (2) packstone; and (3) grainstone. The syndepositional diagenetic processes, such as micritization, caused the formation of mouldic and vuggy pores by dissolution of the allochems. Some of the vugs and moulds were further cemented by sparry calcite and/or microspar. Dolomitization was also observed with some of the micrite and sparite being altered to dolomite. The main diagenetic events observed in the S Field are comparable to other Miocene carbonate reservoirs in the Central Luconia Province (Epting 1980; Janjuhah *et al.* 2017*b*) and the East Natuna, Sarawak Basin (Dunn and Kozar 2006). In general, the evolution of reservoir properties in these Miocene carbonate build-ups is primarily controlled by a combination of early depositional fabric and multistage diagenetic overprinting. Early marine and near-surface diagenesis include micritization, marine cementation and early lithification, which locally stabilize framework grains but can reduce primary intergranular porosity. Subsequent subaerial exposure and freshwater phreatic diagenesis promote selective dissolution of metastable carbonate phases (e.g. aragonitic corals and skeletal grains), leading to the development of secondary porosity types such as mouldic, vuggy and intraparticle porosity that significantly enhance reservoir quality. With progressive burial, mechanical compaction and pressure solution increasingly reduce porosity and permeability, particularly in finer-grained or mud-supported facies, while burial cementation further occludes pore space. Dolomitization, where present, may either enhance permeability through intercrystalline pore networks or degrade reservoir quality where dolomite acts as pore-filling cement, increasing microporosity and reducing effective permeability. The relative importance of these processes varies systematically with depositional facies, burial depth and fluid-flow history, resulting in strong vertical and lateral heterogeneity in porosity and permeability at both core and field scales.

Mineralogical composition of carbonate reservoir rocks

Based on the mineralogical composition of the different stratigraphic units, distinct CO_2WRI can be hypothesized. The calcite-dominated gas zones are expected to exhibit rapid initial buffering of CO_2-induced acidity through carbonate dissolution, potentially leading to short-lived changes in pore structure but limited long-term reactivity once near-equilibrium conditions are attained. In contrast, the calcite–dolomite assemblage of the aquifer zone may display slower reaction kinetics, with dolomite dissolution expected to be more limited under the prevailing high-temperature conditions. The clay-rich caprock units (Seals A and B), dominated by illite and mixed-layer illite–smectite with only minor reactive carbonate phases, are anticipated to show minimal mineralogical reactivity over experimental timescales, with any CO_2 interaction primarily affecting pore fluids rather than the solid framework. These hypotheses provide a framework for assessing the experimental observations presented below.

As such, the mineralogical composition of the reservoir determines rock reactivity with reservoir fluids and the injected CO_2 (Solomon 2006). X-ray diffraction analysis was performed on 38 carbonate powder samples from various depths in well S-4 (Fig. 6). Results from gas zone samples show that calcite is the dominant mineral type, averaging 80 wt%. Small amounts of dolomite, plagioclase, K-feldspar, pyrite, quartz and clay were also identified. In contrast, dolomite and calcite co-dominate the aquifer zone, with ~40 and ~50 wt% respectively. Both gas and aquifer zones contain illite and illite/smectite mixed layers as the main clay minerals, but in very small quantities. Detailed XRD results are summarized in the Supplementary material (SI 3).

Carbonates in the gas zone of the S Field were deposited in a reef environment with the presence of algae and planktonic foraminifera along with corals. This probably resulted in the formation of high calcite carbonates. For the aquifer zone, however, the carbonate rock is interpreted to be deposited in a lagoonal environment. This reflects the co-occurrence of calcite and dolomite. The formation of dolomite could be related to a sea-level rise during the deposition of carbonate in the present-day aquifer zone. Exposure of carbonates to meteoric waters during sea-level drop may have caused unstable

Downloaded from http://pubs.geoscienceworld.org/gsl/geoenergy/article-pdf/doi/10.1144/geoenergy2025-046/7859514/geoenergy2025-046.pdf by TU DelftLibrary user on 10 J

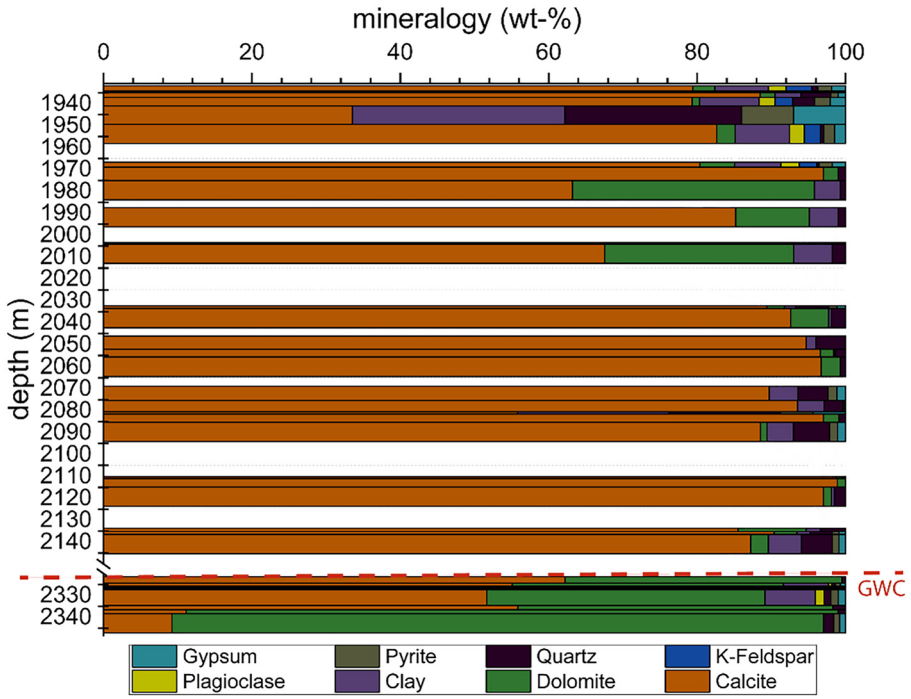


Fig. 6. Distribution of mineral composition in the carbonate reservoir. Gas water contact (GWC) separates the gas zone from the aquifer zone.

minerals to dissolve (Moore 1989). Higher dolomite contents with smaller grain sizes in the aquifer zone may be due to the breakup of small planktonic foraminifera such as Globigerina (Chave 1961). In addition, we can speculate that the difference in mineralogy between the aquifer and the gas zones is partly due to differences in hydrodynamics whereby the gas zone is disconnected from basinal flow systems with limited or no exchange of reservoir fluids, resulting in limited reservoir diagenesis. Again, this is in addition to high gas saturations in the gas zone and therefore limited formation brine volumes controlling diagenetic processes. High solution temperatures might have also influenced the precipitation of dolomite in the aquifer, whereas the lower temperature in the gas zone may have resulted in calcite replacement (Morad *et al.* 2018).

Caprock properties and significance for CO_2 storage

Capillary entry pressure and column height of caprock Seal A

The capillary entry pressure is an important parameter to evaluate the sealing capacity of caprocks (Krushin 1997; Divko *et al.* 2010; Busch and Amann-Hildenbrand 2013; Fatah *et al.* 2020). Five samples from Seal A have been tested by mercury intrusion capillary pressure (MICP) analysis, providing information on porosity and most prominent pore sizes (Table 3).

From MICP data, maximum gas column heights can be estimated (Busch and Amann-Hildenbrand 2013), ranging between 583 and 753 m. This is based on a gas density taken at initial reservoir conditions with P_{CO2} of 70%, CO_2 interfacial tension (IFT) of 20 mN m^{-1} (Busch *et al.* 2013) and assuming a contact angle of 0° (water-wet conditions). The pore throat size is the main control on capillary entry pressure calculation and column height estimation. A difference of 4 nm on average pore radius between samples S-4 A2 and S-4 A3 results in 170 m of additional column height. The calculated CO_2 seal capacity for Seal A from this study is higher by about 300–450 m, compared to the current gas column height in the reservoir which is ~300 m. The calculation uses 0° for the contact angle, although there is a possibility of a non-zero contact angle (Iglauer *et al.* 2015). A sensitivity analysis on the contact angle has been conducted with the angle ranging from 0 to 35° and results show a decreasing gas column height with an increase in contact angle by about 100 m, which still does not exceed the current column height in the S Field of 300 m. Therefore, based on this evaluation, the risk of having capillary CO_2 leakage into the caprock is considered low.

Permeability of Seal A (primary caprock)

Measurement of pulse decay gas permeability under *in situ* stress conditions has been conducted on one Seal A sample, revealing a permeability of 0.5 µD and a porosity of 2.4%. The porosity value is consistent with the measured porosity obtained from MICP on sample S-4 A3, which is from the same depth. The pulse decay measurement was repeated three times using different initial pressures. In addition, the sample has been dried prior to unconfined gas permeability testing, possibly resulting in dehydration and therefore shrinkage of swelling clays, or possibly into the formation

Table 3. Results of MICP measurements for five samples from Seal A

Sample ID		S-4 A2	S-4 A3	S-4 A4	S-4 A5	S-4 A6
Sample depth	m	1853.3	1853.2	1850.5	1851.8	1858.4
MICP porosity	%	6.2	2.2	10.0	10.0	10.0
Most prominent pore radius	nm	11	9	10	10	10
Interfacial tension	mN m^{-1}	20	20	20	20	20
Contact angle	°	0	0	0	0	0
CO_2 capillary entry pressure	MPa	3.5	4.5	4.0	4.0	4.0
CO_2 column height	m	583	753	670	670	670

Downloaded from http://pubs.geoscienceworld.org/gsl/geoenergy/article-pdf/doi/10.1144/geoenergy2025-046/7859514/geoenergy2025-046.pdf by TU DelftLibrary user on 10 J

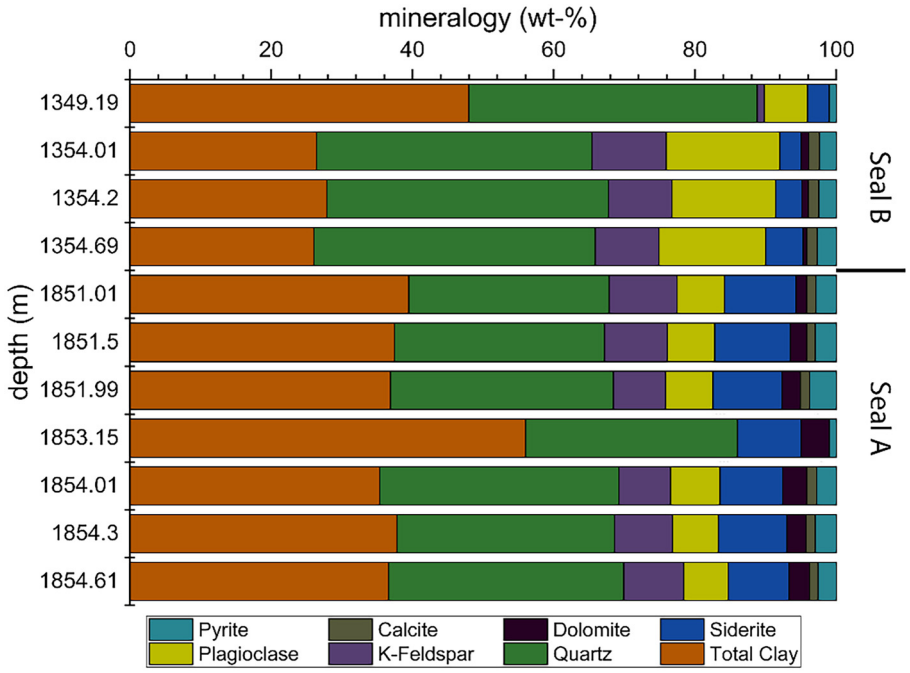


Fig. 7. Distribution of mineralogy in shale samples of Seal A and Seal B from the S-4 well in their initial state.

of microfractures. As a result, the value should be treated with great care and only used as an upper limit of the true, *in situ* permeability. This concern is substantiated when applying the Yang and Aplin (2007) permeability model, which is based on clay content, porosity and mean pore throat radius. For samples S-4 A2 and S-4 A3 we obtain porosities of 6.2 and 2.2% and mean pore throat radii of 11 and 9 nm, respectively. Clay content from the same depth (1853 m) was determined at 56%. This clay value, however, is high in comparison to overlying and underlying layers which are ~36%. Calculating permeability from the Yang and Aplin (2007) model provides a permeability between 1 and 4 nD ($1–4 \times 10^{-21}$ m^2) and therefore two orders of magnitude lower than provided by the unconfined method.

It should be noted that the permeability measured on intact shale core plugs is interpreted to represent matrix-dominated flow at the centimetre scale, whereas effective permeability at the formation scale may be higher if connected fractures or discontinuities are present. However, the laterally continuous depositional character, mineralogical homogeneity and lack of evidence for pervasive natural fracturing in Seal A suggest that matrix permeability remains the dominant control on large-scale fluid flow.

Mineralogical composition of Seals A and B

Seal A (primary caprock) has slightly higher average clay contents compared to seal B (secondary caprock) (Fig. 7). The clay mineralogy of the caprock layers is mainly characterized by illite, followed by mixed-layer illite–smectite, kaolinite, smectite and chlorite. Furthermore, siderite contents are lower and plagioclase contents higher in Seal B compared to Seal A. The heterogeneity of the caprock samples was determined through analyses of eight Seal A and four Seal B samples from the same depths and found to be homogeneous (Dewhurst *et al.* 2020).

CO_2–water–rock interaction

Even though the dissolution of CO_2, potentially followed by mineral carbonation, may offer secondary CO_2 trapping over longer timescales, the impact of this reaction on the degradation of the formation properties can be of concern. Previous studies revealed that CO_2 injection into a subsurface formation may trigger changes in rock and fluid properties, including geochemistry, mineralogy, porosity, permeability and rock strength (Luquot and Gouze 2009; Sterpenich *et al.* 2009; Hangx *et al.* 2010*a*, *b*, 2015; Grgic 2011; Vialle and Vanorio 2011; El Hajj *et al.* 2013; Falcon-Suarez *et al.* 2017; Busch *et al.* 2020; Fatah *et al.* 2020; Busch *et al.* 2023). Therefore, it is important to evaluate the impact of CO_2WRI in the S Field for appropriate assessment of the feasibility and potential subsurface risks.

Based on a simulation study, CO_2WRI in the aquifer zone of the S Field are considered low due to natural saturation of formation waters with CO_2 (Amin and Jaafar 2016). However, at the time, information on the S Field rock and fluid properties was limited, requiring a re-evaluation based on a new core acquired in 2017. Therefore, we here attempt to determine the impact of CO_2WRI on petrophysical (porosity, permeability) and geomechanical properties of the reservoir and caprock. Changes in mineralogical and geomechanical properties of caprock samples have been published previously (Dewhurst *et al.* 2020). A brief summary is provided below, but refer to the original study for full details.

Static batch experiments and impact on petrophysical and mechanical rock properties

CO_2WRI in the carbonate reservoir (aquifer zone) and caprock Seal A of S-4 well were investigated in detail using an integrated experimental approach. A representative composition of the formation water in the S Field was formulated to prepare a synthetic brine (Table 1). Pressures and temperatures used in the experiment are similar to the original reservoir conditions of the S Field.

The impact of the injected CO_2 is variable throughout operations, either during the CO_2 injection phase with timescales on the order of tens of years, or after CO_2 injection with timescales of hundreds to thousands of years. This reflects interactions between the injected CO_2 and reservoir fluids/rocks, which depend on the distance from the injector where reservoir fluid-water–rock equilibria are significantly disturbed over distances of several hundreds of metres (depending on reservoir porosity, permeability and injection rates).

Static batch experiments were performed to simulate the scenario representing the far field of the reservoir, where CO_2 dissolution in formation fluids and dissociation decreases pH (Pokrovsky *et al.*

Downloaded from http://pubs.geoscienceworld.org/gsl/geoenergy/article-pdf/doi/10.1144/geoenergy2025-046/7859514/geoenergy2025-046.pdf by TU DelftLibrary user on 10 J

2005). This changes the geochemical equilibrium, triggering reactions between CO_2, brine and rock, depending on mineralogy, formation water composition, pressure and temperature (Kaszuba *et al.* 2011; Dawson *et al.* 2013). We performed static batch experiments to obtain input for predicting the integrity and safety of CO_2 storage in the S Field over a long period of time. These experiments were selected to represent far-field conditions where transport is diffusion-dominated and fluid–rock systems progressively approach equilibrium; in contrast, flow-through configurations maintain a stronger disequilibrium driving force and are more representative of near-injector conditions, but are difficult to implement for intact caprock due to capillary entry constraints and very low achievable flow rates.

Core chips from the water zone, gas zones B and C as well as Seals A and B from well S-4 were used for CO_2WRI. The core chips were subdivided into four batches for XRD, XRF, specific surface area (SSA) and cation exchange capacity (CEC), respectively. Experiments were conducted for four different time periods: unreacted ('pre') samples and reacted samples after exposure to carbonated fluids ('post') for one, four and six months. These CO_2 ageing experiments were conducted in high pressure vessels and at 150°C and a pressure of ~29 MPa with one pore fluid volume of synthetic brine present; samples were pressurized using supercritical CO_2.

Carbonate reservoir. The results of the XRD analysis on samples from the aquifer zone are shown in Table 4. The rock in its initial state (0 months) is dominated by dolomite and calcite (with trace amounts of quartz, clay minerals, halite and svanbergite of <3% in total). Clay minerals are mainly composed of illite–smectite mixed layers and smectite (data not shown here). From the results, ageing in supercritical CO_2 for one, four and six months shows no clear impact on the mineralogy of the rock. The minor variations are close to the level of accuracy for the technique and may be due to rock sample heterogeneity.

In line with the observed mineralogical changes, the variation in elemental composition (especially CaO and MgO) is small and mostly within the experimental uncertainty of the analysis (Supplementary material, SI 4). A small decrease in SiO_2, Al_2O_3, Fe_2O_3 and SO_3 was observed over time in the aquifer zone, possibly indicating partial dissolution of clay minerals. This is however not confirmed from XRD analysis, probably due to the relatively large error margins associated with trace mineral phases.

The mineralogical composition of gas zone samples B and C from the S Field differs significantly from the aquifer zone with notably higher calcite contents (~97 and 88 wt% respectively) and minor amounts of other mineral phases such as dolomite, pyrite, dickite and gypsum. However, similar to the aquifer zone, the static ageing for one, four and six months shows no mineralogical change (Table 4). In terms of geochemical composition, CaO is obviously the main element (~54%), consistent with calcite being the primary mineral phase. Other elements are present at <1% in gas zone B samples, while SiO_2 and Al_2O_3 are slightly more elevated in gas zone C samples, probably due to higher clay contents. Again, no significant changes in elemental composition were observed following CO_2 exposure for up to six months.

Table 4. Mineralogical changes of aquifer and gas zones B and C samples following CO_2WRI under in situ conditions

Time (months)	Calcite	Dolomite
	Aquifer zone	
0	44.0	54.0
1	43.5	55.0
4	44.0	54.0
6	47.0	51.5
	Gas zone B	
0	97.0	2.0
1	97.0	2.0
4	98.0	2.0
6	97.0	2.0
	Gas zone C	
0	88.5	2.0
1	88.0	2.0
4	88.0	2.0
6	89.0	2.0

The minimal CO_2WRI observed suggests that the carbonate formation in the S Field is already at or near to equilibrium with dissolved CO_2 in formation waters. As a result, further geochemical changes are either unlikely or occur beyond the six-month experimental time frame used in this study. Similar results have been reported through high resolution analyses of subsequent experiments, using samples from the same zones under comparable conditions (Sazali *et al.* 2019). Several studies have investigated CO_2WRI in carbonate samples under batch conditions, which are like the scenario studied here (Gunter *et al.* 2000; Kaszuba *et al.* 2011; Dawson *et al.* 2013; Siqueira *et al.* 2017). However, none of these studies were conducted under the high-pressure and high-temperature conditions applied in our experiments. Findings from previous studies indicate non-linear changes in ionic species concentration over time, a small increase in porosity and no significant change in mineralogy or mechanical properties (Dawson *et al.* 2013). Carbonate minerals are reactive minerals that tend to dissolve rapidly at low pH as the kinetic rates are fast (with magnitudes of 10^{-7} mol m^{-2} s^{-1}) compared to other minerals such as illite (10^{-13} mol m^{-2} s^{-1}) or quartz (10^{-14} mol m^{-2} s^{-1}) (Zhang and Wu 2018). Thus, mineral dissolution is more likely in carbonate samples. Previous findings further suggest that the rapid dissolution of calcite will result in a short time for the reaction to achieve an equilibrium state. However, pH buffering effects will influence the reaction of carbonate minerals (Grgic 2011). This has been suggested by static batch experiments on different limestone samples dominated by calcite, which show slight changes in mineral and fluid geochemical composition (Sterpenich *et al.* 2009; Rimmelé and Renard 2010; Berrezueta *et al.* 2017). Batch experiments were also conducted on the carbonate samples from the IEA Weyburn CO_2 storage site, and it was concluded that geochemical reactions did not reduce the porosity and permeability of the carbonate formation (Riding and Rochelle 2009). The high native CO_2 content of the S Field reservoir indicates that reservoir rocks and formation fluids have been exposed to elevated CO_2 partial pressures over geological timescales (millions of years). Such prolonged exposure is expected to drive the system towards geochemical equilibrium, thereby limiting ongoing mineral reactivity. The minimal mineralogical, petrophysical and geomechanical changes observed in our laboratory experiments are therefore consistent with a reservoir that has already undergone long-term CO_2–water–rock interaction prior to any engineered CO_2 reinjection. This is also valid for the caprock discussed below.

In addition, this is consistent with field analogue studies which show that CO_2 exposure did not change the mineral composition (Xiao *et al.* 2011; Bickle *et al.* 2013; Heinemann *et al.* 2013; Busch *et al.* 2014; Hangx *et al.* 2015). Additionally, high CO_2 saturation conditions prevent mineral precipitation, supporting the stability of the system. Thus, additional CO_2 injection into the water zone is unlikely to cause major impact on reservoir properties, such as porosity and permeability.

Caprock. Static batch experiments were also conducted on caprock samples to evaluate the potential enhancement of matrix permeability if the injected CO_2 migrates by advection or diffusion into the caprock. It has previously been reported by Dewhurst *et al.* (2020) that reaction of Seals A and B with CO_2 does not lead to significant mineralogical changes. In that study, multiple samples

Downloaded from http://pubs.geoscienceworld.org/gsl/geoenergy/article-pdf/doi/10.1144/geoenergy2025-046/7859514/geoenergy2025-046.pdf by TU DelftLibrary user on 10 J

from Seals A and B were tested to determine the degree of homogeneity to establish a baseline from which the significance of any changes in mineralogy could be evaluated. The initial whole rock composition for Seal A is dominated by quartz (~30%) and clay minerals (~55–60%), with kaolinite, mixed layer illite–smectite (85–90% illite) and illite dominating the clay fraction. In addition, Fe-bearing siderite is a significant component (~10%) and some minor amounts of dolomite and ankerite are present. Seal B is dominated by quartz (~40%), clay minerals (~27%) and feldspar (~25%). The clay fraction is composed of mixed layer illite–smectite (70–80% illite), smectite (5–8%), illite, kaolinite and some chlorite.

Mineralogy is an important caprock property that influences the impact of CO_2WRI on caprock sealing capacity (Busch *et al.* 2010). From previous studies, the occurrence of smectite with chlorite may be converted to illite in the presence of CO_2 (Alemu *et al.* 2011). A study on the impact of CO_2 exposure to Eau Claire shale by (Liu *et al.* 2013) revealed dissolution of feldspar and anhydrite associated with precipitation of pore-bridging illite and smectite, as well as minor precipitation of siderite adjacent to pyrite. A flow-through experimental study conducted on a caprock sample from a CO_2 storage site at In Salah, Algeria, found that CO_2WRI resulted in increased permeability and porosity by dissolution of siderite and chlorite (Armitage *et al.* 2013).

However, this was not observed in the Dewhurst *et al.* (2020) study and no significant mineralogical changes were found. This is expected, as reactive minerals such as carbonate only occur in minor amounts and reaction rates for other minerals (mainly silicates) are significantly lower and probably outside the timescales that can be reproduced under laboratory conditions and using a single pore volume of formation fluid for reaction with CO_2 and the rock.

Geomechanical properties (pre- and post-CO_2 ageing)

Any changes in poroelastic behaviour, whether in the caprock or reservoir rock, may trigger mechanical damage such as wellbore breakouts, fault (re)activation, formation fracturing or reservoir compaction. Geomechanical risks associated with geological CO_2 storage decrease away from the wellbore due to pore pressure reduction into the far field. However, the effects of chemical reactions must also be evaluated (Hawkes *et al.* 2005). Previous studies revealed that the impact of CO_2WRI on the geomechanical properties may be influenced by mineralogy, pH, permeability and porosity (Hangx *et al.* 2013, 2015; Zheng *et al.* 2015). Porosity reflects the amount of water that is in contact with the rock. The water–rock ratio will influence the geochemical interaction between reactive fluids and the mineralogy of the rocks (Hangx *et al.* 2015).

In this study, we conducted two types of laboratory tests to study the effect of chemomechanical impact on caprock and reservoir samples from the S Field. These tests were single-stage triaxial tests and Brazilian tensile strength tests. The principal stresses, tensile stress, elastic properties (Young's modulus, Poisson's ratio) and failure criteria were used to validate the geomechanical properties generated by well logs in a one-dimensional geomechanical model. To assess the impact of CO_2WRI, we compared geomechanical properties pre- and post-CO_2 exposure. Representative twin core samples from each zone in well S-4 were selected from the same depth to obtain similar rock properties in terms of mineralogy and porosity, and therefore to minimize heterogeneity effects on test results. All samples were photographed and CT scanned before testing to confirm the absence of internal or pre-existing (micro-)fractures. Porosity and permeability measurements were also conducted on the carbonate samples to establish petrophysical properties.

For the carbonate samples, the consolidated drained (CD) triaxial method has been used to avoid excess pore pressure during the shearing phase (Addis *et al.* 2012; Rees 2013). This test describes long-term loading responses, providing strength parameters determined under effective stress control. A different method is used for the shaly caprock samples, which is a consolidated undrained (CU) experiment, where pore fluids are not allowed to drain from the sample (Josh *et al.* 2012; Dewhurst *et al.* 2015; Ewy 2018; Giger *et al.* 2018). CU tests allow strength parameters to be determined based on effective stresses.

In situ pressure and confining stress magnitudes were chosen based on the field conditions. Different confining stresses were used during triaxial testing for each sample, ranging from higher to lower *in situ* stresses to evaluate the strength behaviour and the failure envelope. During the shearing stage, the confining stress and pore pressure were monitored and kept constant throughout the carbonate sample testing. For the shale samples, only the confining stress was maintained but not the pore pressure, since excess pore pressure is dynamic during undrained experiments. The differential stress between the axial load applied and confining stress was recorded. The effective normal stress σ_n' is obtained by subtracting the pore pressure P_p from the normal stress σ_n.

Strength or rock failure can be interpreted by stress and strain criteria. The principal stress σ_1, or the maximum stress, is represented by the total axial stress (axial load plus confining pressure) and σ_3, or the minimum stress, is given by the confining stress. The stress–strain curve is plotted to determine the peak strength of the samples. Young's modulus E is calculated by taking the slope of the differential stress-axial strain curve at 40 to 60% of the peak strength. Poisson's ratio ν was estimated by plotting the axial against the radial strain with the same range of axial strain used for E. However, the preserved shale samples exhibited non-linear stress–strain behaviour in the 40–60% range of peak strength. Therefore, elastic properties were calculated within the linear portion of the curve between ~2 and 10 MPa differential stress. The classical Mohr–Coulomb failure criterion was applied to evaluate strength parameters.

Carbonate reservoir. In general, mineralogy and porosity are key factors influencing rock strength; changes in these can lead to formation weakening, reservoir compaction and ultimately porosity reduction (Busch *et al.* 2023). However, heterogeneities caused by diagenetic processes, such as grain-to-grain contacts and pore type variations, can also have a major contribution (Hangx *et al.* 2015). Thus, detailed characterization of composition, texture and porosity is essential for evaluating any potential CO_2 storage reservoir (Busch *et al.* 2014; Hangx *et al.* 2015). Most previous studies on the effect of CO_2WRI on mechanical properties have focused on sandstone reservoirs (e.g. Hangx *et al.* 2015). Therefore, limited published data are available for carbonate systems, making direct comparisons with the findings from this study more challenging.

We used 12 representative carbonate samples from the gas zone and six carbonate samples from the water zone for triaxial testing. Samples were divided into two batches to evaluate the rock mechanical property changes due to CO_2 exposure.

Initial porosity and permeability as well as stress/pressure data for single-stage triaxial testing are provided in Table 5. The porosity and permeability of carbonate samples from each zone are different. Average porosity for samples from gas zone B is 30% and average permeability is 180 mD. Slightly higher average porosities and permeabilities from gas zone A have been determined (~36% and ~350 mD respectively). Samples from the water zone show the lowest values for average porosity (~28%) and average permeability (~30 mD). In terms of rock composition and fabric, both gas zone samples mainly consist of calcite (>90 wt%) with heterogenous vuggy and mouldic pore structures.

The unreacted set of carbonate samples used for triaxial testing originates from the production gas zone B, at a depth of between 1973.10 and 1973.63 m. The lowest *in situ* pore pressure used is 34.6 MPa, relating to the shallowest sample depth for carbonate reservoir zones. Stress–strain curves show different behaviour for

Downloaded from http://pubs.geoscienceworld.org/gsl/geoenergy/article-pdf/doi/10.1144/geoenergy2025-046/7859514/geoenergy2025-046.pdf by TU DelftLibrary user on 10 J

Table 5. Sample properties and setup for triaxial testing of samples from the gas and water zones with porosity, permeability, peak/yield stress, Young's modulus and Poisson's ratio

Zone and test condition	Depth, m	Sample ID	Porosity %	Permeability, mD	Initial confining stress MPa	Initial pore pressure MPa	Peak or *yield stress MPa	Young's modulus GPa	Poisson's ratio
Gas zone B (initial)	1973.10	2527	32.0	165	39.0	34.6	*14.0	4.2	0.24
	1973.60	2529	29.0	195	45.0	34.6	*16.0	5.3	0.17
	1973.63	2530	30.0	212	50.0	34.6	*11.0	2.5	0.09
Gas zone B (after CO_2WRI)	1973.10	2683	32.4	183	39.0	34.8	7.5	2.2	0.25
	1973.58	2688	30.9	252	45.0	34.7	7.6	3.2	0.25
	1973.69	2689	29.9	167	50.0	34.7	5.8	4.7	0.41
	1973.58	2687	33.0	84	55.0	34.7	3.1	3.0	0.28
Gas zone A (initial)	2110.47	2635	34.0	249	40.5	35.2	10.4	4.0	0.28
	2110.64	2637	37.0	353	50.5	35.2	*4.4	4.0	0.19
	2110.64	2642	37.0	326	60.5	35.2	*7.7	1.8	0.13
Gas zone A (after CO_2WRI)	2110.93	2637	34.5	237	40.5	35.2	8.7	3.8	0.40
	2110.93	2642	37.8	574	50.5	35.2	*2.2	2.3	0.26
Water zone (initial)	2328.20	2507	28.5	34	40.0	36.5	27.0	8.6	
	2328.20	2506	28.3	30	43.7	36.7	31.0	8.4	0.24
	2328.10	2505	27.2	27	55.0	36.6	40.0	9.2	0.19
Water zone (after CO_2WRI)	2330.70	2705	29.1	33	40.0	36.7	14.5	5.4	0.21
	2330.55	2703	28.6	30	43.7	36.7	21.6	6.1	0.33
	2330.55	2701	28.6	33	55.0	36.7	19.3	5.8	0.25

Core plugs with similar properties have been selected to represent each zonation. Initial confining stress and pore pressure have been selected based on the *in situ* pressure at the respective sample depth. Peak or yield stress is dependent on whether the samples in question showed strain softening (brittle), pure ductile or strain hardening behaviour (see Fig. 8).

each sample without clear correlation to confining pressure (Fig. 8a). Some of the lower porosity samples are brittle and show a clearly defined peak stress at the maximum of the stress–strain curve. However, some samples are ductile or strain harden so a yield stress is defined at the departure from linearity on the stress–strain curves (e.g. Baud *et al.* 2009; Cilona *et al.* 2012). As a peak strength is often not defined, in these cases the elastic range used to calculate E and ν is taken at low differential stress on the linear part of the stress–strain curve.

The sample tested under the lowest effective confining pressure at ~5 MPa shows ductile behaviour and a yield stress constant at 14 MPa. The strongest sample, with a yield stress of 16 MPa, shows strain hardening after the yield point at 19 MPa. The third sample was tested at the highest effective confining pressure of ~15 MPa. No peak stress was recorded, and strain hardening identified as the dominant effect after yield stress of 11 MPa. E and ν for these samples were calculated from the linear stress interval before yield. The range of initial E for gas zone B is 2.5–5.3 GPa and ν ranges between 0.09 and 0.24. These differences suggest the influence of carbonate rock heterogeneity on mechanical strength. The heterogeneity can be caused by the pore types, cement types, biological components and microcracks (Eberli *et al.* 2003; Ajalloeian *et al.* 2017).

The second set of carbonate samples from gas zone B includes samples following ageing with supercritical CO_2 for 35 days under *in situ* reservoir pressure and temperature conditions. The initial confining stress and pore pressure used is the same as for the first set of samples at initial conditions. Stress–strain curves show different strain hardening behaviour for almost all samples without clear correlation to the confining pressure (Fig. 8b). Sample 2683, tested with the lowest effective confining pressure at ~5 MPa, shows a peak stress at ~11 MPa with stable residual strength at ~10 MPa towards the end of the test. The other three samples show strain hardening behaviour without any peak stress. The same approach was used to calculate Young's modulus E and Poisson's ratio ν compared to samples at initial conditions (without ageing). The range in E is 2.2–4.7 GPa and 0.25–0.41 for ν.

In total, six core plug samples from gas zone A were prepared for triaxial testing. Three unreacted samples were used for initial characterization of rock strength properties. Effective stress conditions for this set of samples were chosen using higher initial confining stress and pore pressure conditions compared to gas zone B, considering a greater sample depth of ~2100 m. The initial confining stress applied was ~40, ~50 and ~60 MPa with an initial pore pressure of ~35 MPa. Each sample shows an individual trend of stress–strain curve (Fig. 8c). Sample 2635 was tested at lowest confining stress (~5 MPa) and was the only sample showing shear failure with a peak strength at 10.4 MPa. In contrast, the second and third sample tested with higher confining stresses show strain hardening with yield strengths at 4.4 and 7.7 MPa respectively. E for this set of samples ranges from 1.8 to 4 GPa and ν from 0.13 to 0.4.

One sample dedicated to post-CO_2 ageing was damaged before testing. Thus, only two samples were available for testing under low and medium confining stresses. Peak stress at 8.7 MPa was observed from the stress–strain curves of sample 2637, while a small peak stress of 2.2 MPa was recorded from the stress–strain curve of sample 2642, followed by strain hardening in the residual strength phase (Fig. 8d). Elastic properties for these post-CO_2 ageing samples are similar to unreacted samples, with E ranging between 2.3 and 3.8 GPa and ν between 0.26 and 0.4.

Three carbonate samples from the aquifer zone, originating from a depth of 2328.2 m, were used for triaxial testing to determine the unreacted rock strength properties. The lowest effective confining pressure of 3.5 MPa was applied to sample 2507 with constant confining pressure and pore pressure. From the stress–strain curve in Figure 8e, the sample shows brittle behaviour with an increase in peak strength up to ~27 MPa and a decrease to residual strength of ~16 MPa. Samples 2506 and 2505 show higher peak stresses with increasing effective confining pressure of 7 and 19 MPa. The residual strength of sample 2506 is also higher compared to the sample with lower confining pressure (2507). A different scenario is observed for sample 2505, where the peak strength remains constant until the end of the test, suggesting ductile behaviour on the macroscopic scale with slight strain hardening (Fig. 8e). Unreacted E is 8.5–10 GPa. Using the same axial strain interval (linear elastic zone) as for the E calculation, Poisson's ratio ν was calculated to be 0.2 to 0.3. In summary, the stiffness of samples from the S-1 aquifer zone increases with effective stress shown by the increase of E and decrease of ν. Compared to the gas zone, the high E in the aquifer

Downloaded from http://pubs.geoscienceworld.org/gsl/geoenergy/article-pdf/doi/10.1144/geoenergy2025-046/7859514/geoenergy2025-046.pdf by TU DelftLibrary user on 10 J

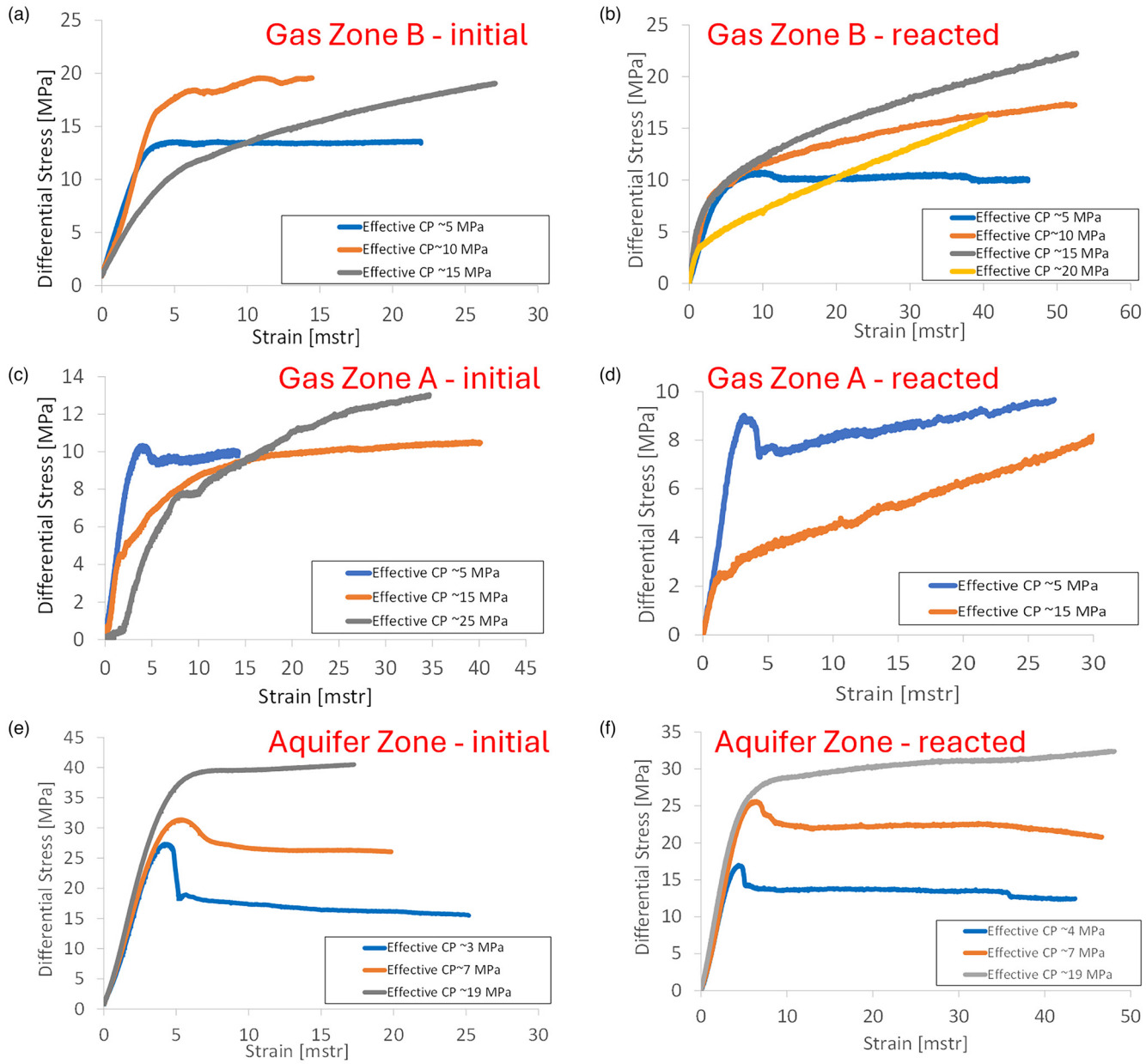


Fig. 8. Stress–strain curves for gas zone B (**a**) unreacted and (**b**) CO_2-reacted samples. Curves show different deformation behaviour of each sample at different effective confining pressures (CP) with no obvious stress dependence. Most samples in (b) show strain hardening and no shear failure, apart from the lowest effective CP sample. Stress–strain curves for gas zone A (**c**) unreacted and (**d**) CO_2-reacted samples. Strain hardening at the two higher CP for unreacted samples can be observed, as well as brittle failure for the lowest CP. CO_2-reacted samples in (d) show no dependence of the deformation behaviour on the effective CP applied, which is similar to other samples from gas zones A and B. Stress–strain curves for aquifer zone (**e**) unreacted and (**f**) CO_2-reacted samples, with different effective CP. For both sets of samples, deformation behaviour shows strong dependence on effective stress. Samples tested under the highest effective stress of ~19 MPa show ductile behaviour with slight strain hardening, while samples at lower effective stress show brittle shear failure.

zone suggests that rock strength and elastic properties are controlled by porosity, pore type, mineralogy and cementation.

The same procedure was used to evaluate rock strength changes due to CO_2WRI in aquifer zone carbonates. Three additional samples from a depth of 2330 m were aged with supercritical CO_2 under reservoir conditions. After 35 days of ageing, these samples were used for triaxial testing under the same stresses and pressures used for the unreacted sample. Stress–strain curves are plotted from the triaxial tests and show the same deformation behaviour compared to the unreacted samples. However, the peak stress and E are slightly lower compared to the unreacted samples. Peak stresses range from 14.5 to 21.6 MPa (Fig. 8f) compared to 27 to 40 MPa for unreacted samples, and E ranges from ~5 to ~6 GPa compared to values of ~8.5 to ~10.0 GPa for unreacted samples (Table 5).

Results for unreacted samples are first compared to evaluate the influence of carbonate heterogeneity on the initial rock mechanical properties for both gas and aquifer zones. Samples from the aquifer zone show highest peak strength and E values, followed by gas zone B and gas zone A.

The differences in rock strength properties and elastic moduli between the gas and the aquifer zones suggest that mineralogical composition, pore type and porosity are key controls. Carbonate rock samples in the aquifer zone are lower in porosity compared to samples in the gas zones. In terms of composition, the mineralogy in the aquifer zone is dominated by calcite and dolomite, whereas calcite dominates samples from the gas zones. The differences in pore type may also play a role in the rock strength as the main pore types in aquifer samples is intergranular, but most samples in gas

Downloaded from http://pubs.geoscienceworld.org/gsl/geoenergy/article-pdf/doi/10.1144/geoenergy2025-046/7859514/geoenergy2025-046.pdf by TU DelftLibrary user on 10 J

zones have mouldic and vuggy pore type. Overall, results are consistent with previous studies conducted for carbonate rocks (Palchik and Hatzor 2000; Baud *et al.* 2004; Chang *et al.* 2006; Palchik 2011; Cilona *et al.* 2012; Najibi *et al.* 2015; Ajalloeian et al. 2017; Zambrano *et al.* 2017; Ghafoori *et al.* 2018). Carbonate rocks with high dolomite content, low porosity and less mouldic or vuggy pore type are stronger compared to carbonates dominated by calcite with high porosity and mouldic and vuggy main pore type.

Most of the carbonate samples tested in this study show strain hardening and no direct peak/yield stress correlation with effective stress. Thus, the shear failure criterion, such as Mohr–Coulomb, is not appropriate for these highly porous and heterogenous carbonates. Typical rock failure behaviour can be described using the Mohr–Coulomb failure criterion, which predicts an increase in yield or peak strength with increasing confining pressure. However, in the case of these porous carbonate samples, the yield strength decreases as confining pressure increases, which may be attributed to grain crushing or pore collapse. As a result, the end cap model might be a more appropriate failure criterion to describe the mechanical behaviour of these rocks, as it accounts for the transition from compactive to dilatant deformation (Fossum and Fredrich 2000; Baud *et al.* 2009; Cilona *et al.* 2012, 2014). The end cap model was constructed using the mean effective stress and differential stress shown in Figure 9. The plot shows the end cap failure envelopes for a set of porous carbonate samples with varying porosity. However, due to the limited number of samples available for each carbonate set in this study, a complete end cap envelope was not defined. Nevertheless, the end cap failure envelope from Cilona *et al.* (2014) in Figure 9 can be a reference for aquifer samples in the initial state (prior to CO_2 ageing) as the porosity for the samples is comparable (28%, with one sample at 32%). Similarly, the Majella grainstone samples from Baud *et al.* (2009) with a porosity of 30% are comparable to gas zone B, making their end cap envelope suitable for comparison.

Comparison of triaxial results for carbonate samples from the gas and aquifer zones shows that CO_2-reacted samples are slightly weaker than the unreacted samples. This difference could also be due to sample heterogeneity (e.g. vuggy porosity distribution between core plugs) as CO_2WRI did not indicate significant mineralogical or porosity changes (Table 4). Moreover, rock strength does not only depend on porosity changes but also on fluids inside the pore space (dry/wet, CO_2 saturation, etc.) (Sterpenich *et al.* 2009; Zhou *et al.* 2009; Rimmelé and Renard 2010). However, this study confirms that massive calcite dissolution is unlikely due to pH buffering and equilibrium of carbonates with CO_2-saturated formation fluids. However, the porosity measurements on samples before and after CO_2 reaction show minimal porosity changes that are all within the experimental uncertainty (<5% relative or <1.5% absolute porosity values).

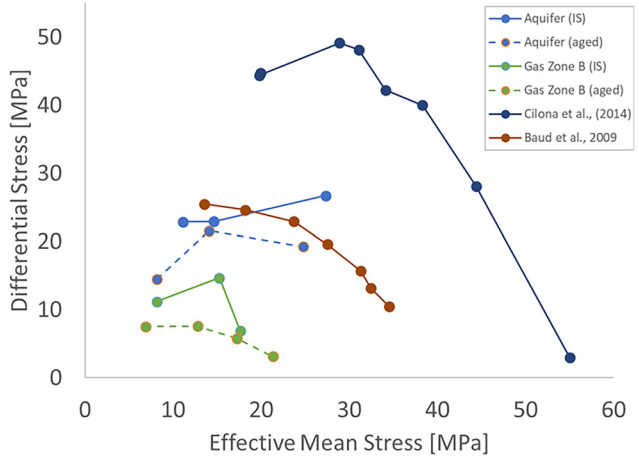


Fig. 9. End cap failure envelopes in the stress space (q–p' space) for initial state (IS) and aged samples from the aquifer zone and gas zone B superimposed on porous carbonate failure data from Cilona *et al.* (2014) and Baud *et al.* (2009). The locations of the end caps in the q–p' space are governed by sample porosity.

The heterogeneity of carbonate rocks makes it difficult to determine reliable rock mechanical properties including tensile strength. Determination of tensile strength can indirectly be obtained from Brazilian tensile strength tests (BTS) or estimated from other rock properties such as uniaxial compressive strength (UCS) (Mellor and Hawkes 1971; Cai 2009; Li and Wong 2013; Nazir *et al.* 2013; Kallu and Roghanchi 2015).

Correlations between BTS and UCS are well established from previous studies, but mostly for clastic rocks. There is limited data for heterogenous carbonate rocks, such as the carbonate formations in the Sarawak Basin. In this study, the tensile strength of the porous carbonates was determined using BTS and UCS, with the latter obtained from laboratory triaxial and core scratch tests and derived from validated 1D geomechanical models.

Porosity is the main index parameter studied and shows a strong relationship with UCS and tensile strength from laboratory tests. Meanwhile, BTS samples with porosities of >30% show tensile strengths of <1.5 MPa. However, higher tensile strengths were obtained from the calculation of one-tenth of the UCS in 1D geomechanical models at the same sample depth and same porosity compared to the tensile strength measured by BTS (PETRONAS, unpublished data). Both correlations between BTS and 1D tensile strength with porosity show a reasonable correlation with an R^2 of 0.7 and are also consistent with empirical equations from the literature (Fig. 10). We therefore conclude that an estimation of tensile strength from BTS and UCS from porosity can be used for high-porosity carbonate samples. This finding is important to ensure that tensile strength data of sensible magnitude are used in geomechanical modelling.

For Brazilian testing, a total of 16 carbonate plug samples were selected from depths closely aligned with those used for triaxial testing to characterize the indirect tensile strength across different carbonate zones and to assess the impact of CO_2WRI. The results reveal that carbonates from the aquifer zone have higher average tensile strengths of ~1.8 MPa compared to those from the gas zones of less than ~1 MPa, with minimal variation observed after CO_2 ageing (Table 6).

These findings suggest that, under the simulated static CO_2 storage conditions, CO_2WRI have negligible influence on the rock strength and elastic properties in the S Field carbonate reservoir. We conducted this series of measurements to evaluate potential long-term changes in mechanical properties away from the injection well, where rocks are not affected by temperature changes and are fully or near-fully water-saturated.

Caprock (Seal A). Twelve representative samples from Seal A, recovered from a depth of 1853 m, were used to determine the geomechanical properties of the effective caprock. We used eight core plug samples for triaxial and four plugs for Brazilian tests. Samples were divided into two batches: the first batch (without CO_2 exposure) was tested to characterize the initial conditions, while the second batch (post-CO_2 exposure) was aged with CO_2 for six months at 29 MPa and 150°C. Results have been published earlier (Dewhurst *et al.* 2020) and show that the samples obtained from Seal A are a relatively weak shale with low cohesive strength (~5 MPa) and low friction coefficient (~0.25). After exposure to supercritical CO_2 for six months, the strength of the samples at each confining pressure stage increased, resulting in small increases in cohesive strength and friction coefficient. Brazilian tests show a low tensile strength normal to bedding of 1.5 to 2.7 MPa when in its preserved state. After exposure to supercritical CO_2 for six months, and resultant loss of pore fluid, the tensile strength has increased to 3.3 to 4.0 MPa.

Downloaded from http://pubs.geoscienceworld.org/gsl/geoenergy/article-pdf/doi/10.1144/geoenergy2025-046/7859514/geoenergy2025-046.pdf by TU DelftLibrary user on 10 J

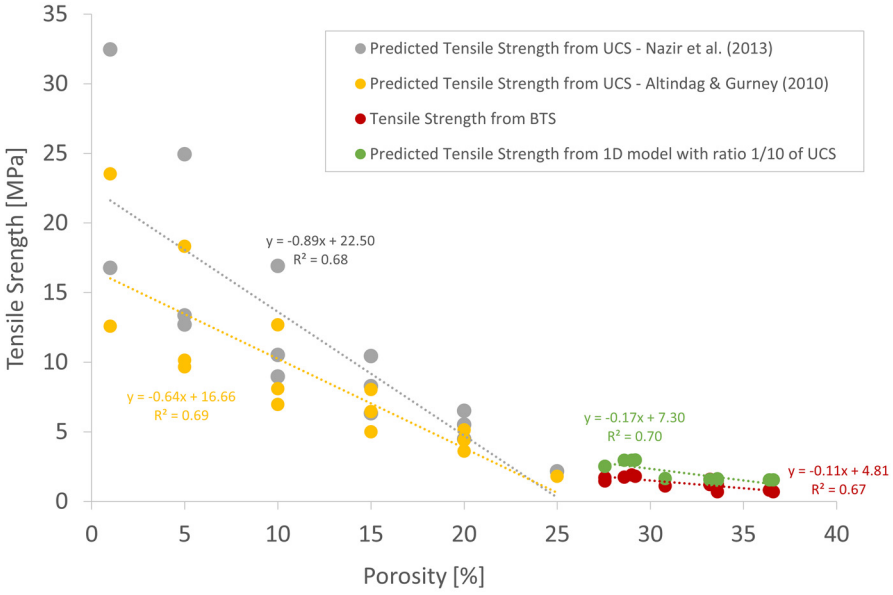


Fig. 10. Tensile strength from Brazilian testing and the 1D geomechanical model shows a decrease in strength with an increase in porosity. The predicted tensile strength from uniaxial compressive strength (UCS) using empirical equations from literature also shows clear correlations with porosity.

Seal A in its initial state has relatively low stiffness with E between ~3 and 6 GPa and Poisson's ratio ν from 0.24 to 0.39. After exposure to supercritical CO_2 and consequent pore fluid loss, the stiffness significantly increases, with E rising to 7.6 to 8.8 GPa and ν decreasing to ~0.15.

There was no change in mineralogy. The increase in strength and stiffness are probably the result of loss of water from the shales, as shown by changes in bulk density and water content (Dewhurst *et al.* 2020). Such effects would probably be limited in the field to the caprock–reservoir interface by capillary considerations and the discrete nature of flow paths in mudrocks with little exposure to reactive fluids.

Implications for CO_2 reinjection into CO_2-contaminated gas reservoirs

Reinjecting CO_2 into the same reservoir from which it is produced represents a distinct and largely untested CCS strategy. This study demonstrates that such an approach can be technically viable and environmentally sound for contaminated gas fields with high CO_2 contents, offering a route to monetize otherwise stranded gas resources under increasingly stringent emission regulations. While this case study is unique for contaminated gas reservoirs, Petrobras is reinjecting CO_2-rich associated gas into the same reservoir for enhanced oil recovery in the Santos Basin, offshore Brazil (Pereira Nunes *et al.* 2024).

The S Field represents a unique case study, whereby the carbonate gas reservoir is highly overpressured and at high temperature. CO_2-rich (~70%) gas would be produced from the gas cap. The gas cap is associated with a calcite-rich facies of the reservoir, whereby CO_2 reinjection will be in the water leg, composed of a mixture of calcite and dolomite. Given the low permeability of the aquifer zone (maximum of 33 mD), it might therefore require more than a single injection well to cover the rates required.

Gas production and CO_2 reinjection will lead to a net decrease in reservoir pressure and therefore a decrease in the risk of leakage because of a decrease in pressure gradient. It should be noted, though, that the net reservoir pressure reduction can still cause fault reactivation, possibly leading to enhanced fault permeability. This is, however, partly compensated for by the CO_2 reinjection, compared to a case where reinjection does not occur into the same hydraulically connected reservoir unit.

Furthermore, as the CO_2 content in the gas leg increases, the interfacial tension is expected to decrease, leading to changes in capillarity within the reservoir and the caprock. For the latter, it is

Table 6. Tensile strength data from Brazilian tests conducted on CO_2-reacted and unreacted carbonates

Zone	Depth m	Porosity %	Indirect tensile strength MPa	Average indirect tensile strength MPa
Gas zone B (initial)	1973.04	33.6	0.7	0.9
	1973.63	30.8	1.1	
Gas zone B (after CO_2WRI)	1973.04	33.7	0.4	0.6
	1973.63	30.4	0.7	
Gas zone A (initial)	2111.55	36.6	0.7	0.9
	2111.55	36.4	0.8	
	2111.73	33.6	1.2	
Gas zone A (after CO_2WRI)	2111.73	35.8	0.5	0.6
	2111.87	35.4	0.7	
	2111.87	34.6	0.5	
Aquifer zone (initial)	2330.28	29.2	1.8	1.8
	2330.49	28.6	1.8	
	2330.62	29.0	1.9	
Aquifer zone (after CO_2WRI)	2330.28	30.3	2.1	1.8
	2330.49	29.0	1.6	

Downloaded from http://pubs.geoscienceworld.org/gsl/geoenergy/article-pdf/doi/10.1144/geoenergy2025-046/7859514/geoenergy2025-046.pdf by TU DelftLibrary user on 10 J

important to balance the decrease in gas column height with a decrease in interfacial tension to evaluate the risk of capillary leakage. A net decrease in methane content in the reservoir will lead to higher solubility of CO_2 in water and therefore to lower pH and possibly some increased reactivity. We tested the reactivity of caprock and reservoir rock material but could not identify any conclusive changes in mechanical, mineralogical or petrophysical properties. This is probably due to the small changes in CO_2 solubility expected and CO_2–water–rock being close to equilibrium in the subsurface already.

A decrease in reservoir pressure and thinning of the gas column will lead to a repositioning of the gas–water contact to a shallower depth and therefore into the calcite-rich facies. This is likely to be followed by water inflow from a connected aquifer and mixing of fresh water with CO_2-charged waters, thereby leading to further CO_2 dissolution and pressure decrease.

Although the S Field is a case study, it presents some key learnings for de-risking similar scenarios for carbon storage. There are many CO_2-contaminated gas reservoirs in the world, and the SE Asia region is known for some of the largest ones. The combination of natural gas production and CO_2 reinjection can lead to a general leakage risk reduction, reduction of costs for exploration, drilling or reservoir and caprock characterization compared to green fields, and might provide additional storage volume beyond the gas production phase due to the pressure space created.

Conclusions

This study provides a comprehensive assessment of the S Field carbonate reservoir and its overlying caprock to evaluate the feasibility and safety of CO_2 reinjection and long-term geological storage. The integrated mineralogical, petrophysical and geomechanical analyses under reservoir conditions demonstrate that both the reservoir and caprock maintain their structural and chemical integrity following exposure to supercritical CO_2.

(1) Reservoir characteristics: the calcite-dominated gas zone exhibits high porosity (>30%) and moderate strength, while the underlying aquifer zone – co-dominated by calcite and dolomite – has lower porosity (20–25%) but higher mechanical strength.
(2) Caprock sealing capacity: Seal A, composed mainly of illite-rich mudrocks and siltstones, has low permeability and high capillary entry pressures, sufficient to retain CO_2 columns exceeding the current reservoir height (~300 m).
(3) CO_2–water–rock interactions: static ageing experiments at 30 MPa and 150°C for up to six months revealed minimal changes in mineralogy, porosity, permeability and mechanical strength in both reservoir and seal samples. The carbonate rocks are already at or near equilibrium with CO_2-saturated formation waters.
(4) Mechanical integrity: no measurable deterioration in elastic moduli or compressive strength was observed post-CO_2 exposure, confirming the mechanical stability of both storage and seal units.

Collectively, these findings indicate a low geochemical and mechanical risk associated with CO_2 reinjection into the S Field reservoir. The system's high-temperature, high-pressure conditions, combined with its mineralogical maturity, contribute to long-term geochemical stability. The results provide a regional analogue for carbonate-hosted CO_2 storage systems in SE Asia and support the viability of reinjecting separated CO_2 streams into the producing reservoir as a safe and cost-effective decarbonization strategy.

Acknowledgements This manuscript has hugely benefited from discussions with various technical people within PETRONAS. We are grateful for their support. Dr Jim Buckman is thanked for his excellent guidance and support in conducting and analysing SEM images. We further thank Mark Trupp and an anonymous reviewer for their constructive comments that significantly improved the content of this paper.

Author contributions **SSMS**: conceptualization (supporting), data curation (lead), formal analysis (lead), investigation (lead), methodology (lead), validation (lead), visualization (lead), writing – original draft (lead); **DND**: formal analysis (equal), investigation (equal), methodology (equal), supervision (supporting), validation (supporting), writing – review and editing (equal); **AG**: formal analysis (equal), investigation (equal), methodology (equal), writing – review and editing (supporting); **MDR**: investigation (equal), methodology (equal), writing – review and editing (supporting); **SSMA**: funding acquisition (supporting), supervision (equal), writing – review and editing (supporting); **SG**: funding acquisition (lead), supervision (supporting), writing – review and editing (equal); **AB**: conceptualization (lead), formal analysis (supporting), funding acquisition (lead), investigation (supporting), methodology (supporting), project administration (lead), supervision (lead), writing – original draft (supporting)

Funding This work was funded by PETRONAS Research Sdn Bhd.

Competing interests This research was sponsored by PETRONAS as part of the PETRONAS Centre of Excellence in Subsurface Engineering and Energy Transition (PACESET), located within Heriot-Watt's Institute of GeoEnergy Engineering. SSMS and SSMA are employees of PETRONAS and all other authors are direct or indirect recipients of the research funding.

Data availability All data generated or analysed during this study are included in this published article (and if present, its supplementary information files).

References

Addis, T., Ewy, R., Makurat, A., Pgc, M.D. and Dudley, J. 2012. Workshop on petroleum geomechanics testing. Paper presented at the 1st Workshop on Petroleum Geomechanics Testing, June 23, Chicago, IL.

Ajalloeian, R., Mansouri, H. and Baradaran, E. 2017. Some carbonate rock texture effects on mechanical behavior, based on Koohrang tunnel data, Iran. *Bulletin of Engineering Geology and the Environment*, **76**, 295–307, https://doi.org/10.1007/s10064-016-0861-y

Alemu, B.L., Aagaard, P., Munz, I.A. and Skurtveit, E. 2011. Caprock interaction with CO_2: a laboratory study of reactivity of shale with supercritical CO_2 and brine. *Applied Geochemistry*, **26**, 1975–1989, https://doi.org/10.1016/j.apgeochem.2011.06.028

Ali, S.H., Poppelreiter, M.C., Saw, B.B., Shah, M.M. and Bashir, Y. 2021. Facies, diagenesis and secondary porosity of a Miocene reefal platform of Central Luconia, Malaysia. *Carbonates Evaporites*, **36**, https://doi.org/10.1007/s13146-021-00682-0

Altindag, R. and Guney, A. 2010. Predicting the relationships between brittleness and mechanical properties (UCS, TS and SH) of rocks. *Scientific Research and Essays*, **5**, 2107–2118, https://academicjournals.org/journal/SRE/article-full-text-pdf/A577CD017017

Ameer Hamza, S.N., Ali, S.S., Wahab, M.A., Rashid, S., Fadzil, M.R. and Widyanita, A. 2012. From imagination to reality. *In:* Long, K.F. (ed.) *Deep Space Propulsion*. Springer, 325–344, https://doi.org/10.1007/978-1-4614-0607-5_18

Amin, S.M. and Jaafar, F. 2016. Reactive transport modelling of CO_2 injection into high CO_2 field. Paper presented at the SPE Asia Pacific Oil & Gas Conference and Exhibition, October, Perth, Australia, https://doi.org/10.2118/182187-MS

Armitage, P.J., Faulkner, D.R. and Worden, R.H. 2013. Caprock corrosion. *Nature Geoscience*, **6**, 79–80, https://doi.org/10.1038/ngeo1716

ASTM 2008. *Standard Test Method for Splitting Tensile Strength of Intact Rock Core Specimens 1 D3967-08*. ASTM International, West Conshohocken, PA.

Baud, P., Klein, E. and Wong, T.-f. 2004. Compaction localization in porous sandstones: spatial evolution of damage and acoustic emission activity. *Journal of Structural Geology*, **26**, 603–624, https://doi.org/10.1016/j.jsg.2003.09.002

Baud, P., Vinciguerra, S., David, C., Cavallo, A., Walker, E. and Reuschlé, T. 2009. Compaction and failure in high porosity carbonates: mechanical data and microstructural observations. *Pure and Applied Geophysics*, **166**, 869–898, https://doi.org/10.1007/s00024-009-0493-2

Berrezueta, E., Kovacs, T. and Luquot, L. 2017. Qualitative and quantitative changes of carbonate rocks exposed to SC CO_2 (Basque-Cantabrian Basin, Northern Spain). *Applied Sciences*, **7**, 1124, https://doi.org/10.3390/app7111124

Downloaded from http://pubs.geoscienceworld.org/gsl/geoenergy/article-pdf/doi/10.1144/geoenergy2025-046/7859514/geoenergy2025-046.pdf by TU DelftLibrary user on 10 J

Bickle, M., Kampman, N. and Wigley, M. 2013. Natural analogues. *Reviews in Mineralogy and Geochemistry*, **77**, 15–71, https://doi.org/10.2138/rmg.2013.77.2

Bing, C.H., Raza, A., Rezaee, R., Nagarajan, R., Hamid, M.A. and Gholami, R. 2015. A screening criterion for selection of suitable CO_2 storage sites. *Journal of Natural Gas Science and Engineering*, **28**, 317–327, https://doi.org/10.1016/j.jngse.2015.11.053

Bolli, H.M. and Saunders, J.B. 1982. *Globorotalia mayeri* and its relationship to *Globorotalia siakensis* and *Globorotalia continuosa*. *The Journal of Foraminiferal Research*, **12**, 39–50, https://doi.org/10.2113/gsjfr.12.1.39

Brace, W.F., Walsh, J.B. and Frangos, W.T. 1968. Permeability of granite under high pressure. *Journal of Geophysical Research*, **73**, 2225–2236, https://doi.org/10.1029/JB073i006p02225

Brown, K., Whittaker, S., Wilson, M., Srisang, W., Smithson, H. and Tontiwachwuthikul, P. 2017. The history and development of the IEA GHG Weyburn-Midale CO_2 monitoring and storage project in Saskatchewan, Canada (the world largest CO_2 for EOR and CCS program). *Petroleum*, **3**, 3–9, https://doi.org/10.1016/j.petlm.2016.12.002

Busch, A. and Amann-Hildenbrand, A. 2013. Predicting capillarity of mudrocks. *Marine and Petroleum Geology*, **45**, 208–223, https://doi.org/10.1016/j.marpetgeo.2013.05.005

Busch, A., Amann, A., Bertier, P., Waschbusch, M. and Krooss, B.M. 2010. The significance of caprock sealing integrity for CO_2 storage. Paper presented at the SPE International Conference on CO2 Capture, Storage, and Utilization 2010, November, New Orleans, LA, https://doi.org/10.2118/139588-ms

Busch, A., Kampman, N. *et al.* 2014. The green river natural analogue as a field laboratory to study the long-term fate of CO_2 in the subsurface. *Energy Procedia*, **63**, 2821–2830, https://doi.org/10.1016/j.egypro.2014.11.304

Busch, A., Hangx, S.J.T., Marshall, J.D. and Wentinck, H.M. 2020. Swelling clay minerals and containment risk assessment for the storage seal of the Peterhead CCS project. *International Journal of Greenhouse Gas Control*, **94**, 102924, https://doi.org/10.1016/j.ijggc.2019.102924

Busch, A., Hangx, S., Vialle, S., Rizzo, R.E. and Kampman, N. 2023. Mechanical weakening of a mudrock seal by reaction with CO_2-charged fluids. *Geology*, **51**, 616–620, https://doi.org/10.1130/G51250.1

Cai, M. 2009. A simple method to estimate tensile strength and Hoek-Brown strength parameter m_i of brittle rocks. In: M. Diederichs and G. Grasselli (eds), ROCKENG09: Proceedings of the 3rd CANUS Rock Mechanics Symposium, Toronto.

Chang, C., Zoback, M.D. and Khaksar, A. 2006. Empirical relations between rock strength and physical properties in sedimentary rocks. *Journal of Petroleum Science and Engineering*, **51**, 223–237, https://doi.org/10.1016/j.petrol.2006.01.003

Chave, K.E. 1961. Factors influencing the mineralogy of carbonate sediments. *Limnology and Oceanography*, **7**, 218–223, https://doi.org/10.4319/lo.1962.7.2.0218

Cilona, A., Baud, P., Tondi, E., Agosta, F., Vinciguerra, S., Rustichelli, A. and Spiers, C.J. 2012. Deformation bands in porous carbonate grainstones: field and laboratory observations. *Journal of Structural Geology*, **45**, 137–157, https://doi.org/10.1016/j.jsg.2012.04.012

Cilona, A., Faulkner, D.R. *et al.* 2014. The effects of rock heterogeneity on compaction localization in porous carbonates. *Journal of Structural Geology*, **67**, 75–93, https://doi.org/10.1016/j.jsg.2014.07.008

Cooper, B.A., Raven, M.J., Samuel, L., Hardjono and Satoto, W. 1997. *Origin and Geological Controls on Subsurface CO_2*. Indonesian Petroleum Association.

Cui, X., Bustin, A.M.M. and Bustin, R.M. 2009. Measurements of gas permeability and diffusivity of tight reservoir rocks: different approaches and their applications. *Geofluids*, **9**, 208–223, https://doi.org/10.1111/j.1468-8123.2009.00244.x

Darman, N. and Harun, A.R. 2006. Technical challenges and solutions on natural gas development in Malaysia. *In*: *The Petroleum Policy and Management (PPM) Project 4th Workshop of the China-Sichuan Basin Case Study*. Petroliam Nasional Berhad Beijing, China.

Dawson, G.K.W., Sidiq, H. *et al.* 2013. *ANLEC Project 3-1110-0101: Review of Laboratory-Scale Geochemical and Geomechanical Experiments Simulating Geosequestration of CO_2 in Sandstone and Associated Modelling Studies*.

Dewhurst, D.N. and Siggins, A.F. 2006. Impact of fabric, microcracks and stress field on shale anisotropy. *Geophysical Journal International*, **165**, https://doi.org/10.1111/j.1365-246X.2006.02834.x

Dewhurst, D.N., Siggins, A.F., Sarout, J., Raven, M.D. and Nordgård-Bolås, H.M. 2011. Geomechanical and ultrasonic characterization of a Norwegian Sea shale. *Geophysics*, **76**, https://doi.org/10.1190/1.3569599

Dewhurst, D.N., Sarout, J., Delle Piane, C., Siggins, A.F. and Raven, M.D. 2015. Empirical strength prediction for preserved shales. *Marine and Petroleum Geology*, **67**, 512–525, https://doi.org/10.1016/j.marpetgeo.2015.06.004

Dewhurst, D.N., Raven, M.D. *et al.* 2020. Interaction of super-critical CO_2 with mudrocks: impact on composition and mechanical properties. *International Journal of Greenhouse Gas Control*, **102**, 103163, https://doi.org/10.1016/j.ijggc.2020.103163

Divko, G., Hamilton, P.J. and Victoria, G. 2010. Evaluation of the regional top seal in the Gippsland Basin: implications for geological carbon storage, Gippsland Basin stratigraphy 80099.

Dunham, R.J. 1962. Classification of carbonate rocks according to depositional textures. *In:* Ham, W.E. (ed.) *Classification of Carbonate Rocks – A Symposium*. AAPG.

Dunn, P.A. and Kozar, M.G. 2006. Application of geoscience technology in a geologic study of the Natuna Gas Field, Natuna Sea, Offshore Indonesia. *25th Annual Convention Proceedings*, Indonesian Petroleum Association, 1996, 117–130.

Eberli, G.P., Baechle, G.T., Anselmetti, F.S. and Incze, M.L. 2003. Factors controlling elastic properties in carbonate sediments and rocks. *Leading Edge (Tulsa, OK)*, **22**, 654–660, https://doi.org/10.1190/1.1599691

El Hajj, H., Odi, U. and Gupta, A. 2013. Carbonate reservoir interaction with supercritical carbon dioxide. Paper presented at the International Petroleum Technology Conference, March, Beijing, China, https://doi.org/10.2523/iptc-16561-abstract

Embry, A.F. and Klovan, J.E. 1971. A Late Devonian reef tract on the Northeastern Banks Island, Northwest Territories. *Bulletin of Canadian Petroleum Geology*, **19**, https://doi.org/10.35767/gscpgbull.19.4.730

Epting, M. 1980. Sedimentology of Miocene carbonate buildups, Central Luconia, Offshore Sarawak. *Geological Society of Malaysia, Bulletin*, **12**, 17–30, https://doi.org/10.7186/bgsm12198002

Ewy, R.T. 2015. Shale/claystone response to air and liquid exposure, and implications for handling, sampling and testing. *International Journal of Rock Mechanics and Mining Sciences*, **80**, 388–401, https://doi.org/10.1016/j.ijrmms.2015.10.009

Ewy, R.T. 2018. Practical approaches for addressing shale testing challenges associated with permeability, capillarity and brine interactions. *Geomechanics for Energy and the Environment*, **14**, 3–15, https://doi.org/10.1016/j.gete.2018.01.001

Falcon-Suarez, I., Marín-Moreno, H., Browning, F., Lichtschlag, A., Robert, K., North, L.J. and Best, A.I. 2017. Experimental assessment of pore fluid distribution and geomechanical changes in saline sandstone reservoirs during and after CO_2 injection. *International Journal of Greenhouse Gas Control*, **63**, 356–369, https://doi.org/10.1016/j.ijggc.2017.06.019

Fatah, A., Bennour, Z., Ben Mahmud, H., Gholami, R. and Hossain, M.M. 2020. A review on the influence of CO_2/shale interaction on shale properties: implications of CCS in shales. *Energies (Basel)*, **13**, 1–25, https://doi.org/10.3390/en13123200

Flügel, E. 2004. *Microfacies of Carbonate Rocks*. Springer.

Fossum, A.F. and Fredrich, J.T. 2000. Cap plasticity models and compactive and dilatant pre-failure deformation. Paper presented at the 4th North American Rock Mechanics Symposium, NARMS 2000, July, Seattle, WA.

Ghafoori, M., Rastegarnia, A. and Lashkaripour, G.R. 2018. Estimation of static parameters based on dynamical and physical properties in limestone rocks. *Journal of African Earth Sciences*, **137**, 22–31, https://doi.org/10.1016/j.jafrearsci.2017.09.008

Giger, S.B., Ewy, R.T., Favero, V., Stankovic, R. and Keller, L.M. 2018. Consolidated-undrained triaxial testing of Opalinusc: results and method validation. *Geomechanics for Energy and the Environment*, **14**, 16–28, https://doi.org/10.1016/j.gete.2018.01.003

Grgic, D. 2011. Influence of CO_2 on the long-term chemomechanical behavior of an oolitic limestone. *Journal of Geophysical Research*, **116**, 1–22, https://doi.org/10.1029/2010JB008176

Gunter, W.D., Perkins, E.H. and Hutcheon, I. 2000. Aquifer disposal of acid gases: modelling of water-rock reactions for trapping of acid wastes. *Applied Geochemistry*, **15**, 1085–1095, https://doi.org/10.1016/S0883-2927(99)00111-0

Hangx, S.J.T., Spiers, C.J. and Peach, C.J. 2010*a*. Creep of simulated reservoir sands and coupled chemical-mechanical effects of CO_2 injection. *Journal of Geophysical Research: Solid Earth*, **115**, 1–23, https://doi.org/10.1029/2009JB006939

Hangx, S.J.T., Spiers, C.J. and Peach, C.J. 2010*b*. Mechanical behavior of anhydrite caprock and implications for CO_2 sealing capacity. *Journal of Geophysical Research: Solid Earth*, **115**, https://doi.org/10.1029/2009JB006954

Hangx, S., van der Linden, A., Marcelis, F. and Bauer, A. 2013. Geological storage of CO_2 at the Goldeneye Field (UK). *International Journal of Greenhouse Gas Control*, **19**, https://doi.org/10.1016/j.ijggc.2012.12.016

Hangx, S., Bakker, E., Bertier, P., Nover, G. and Busch, A. 2015. Chemical-mechanical coupling observed for depleted oil reservoirs subjected to long-term CO-exposure – a case study of the Werkendam natural CO_2 analogue field. *Earth and Planetary Science Letters*, **428**, 230–242, https://doi.org/10.1016/j.epsl.2015.07.044

Hawkes, C.D., McLellan, P.J. and Bachu, S. 2005. Geomechanical factors affecting geological storage of CO_2 in depleted oil and gas reservoirs. *Journal of Canadian Petroleum Technology*, **44**, 52–61, https://doi.org/10.2118/05-10-05

Heinemann, N., Wilkinson, M., Haszeldine, R.S., Fallick, A.E. and Pickup, G.E. 2013. CO_2 sequestration in a UK North Sea analogue for geological carbon storage. *Geology*, **41**, 411–414, https://doi.org/10.1130/G33835.1

Ho, K.F. 1978. Stratigraphic framework for oil exploration in Sarawak. *Geological Society of Malaysia*, **10**, 1–13.

Iglauer, S., Pentland, C.H. and Busch, A. 2015. CO_2 wettability of seal and reservoir rocks and the implications for carbon geo-sequestration. *Water Resources Research*, **51**, 729–774, https://doi.org/ 10.1002/2014WR015553

IPCC 2009. *Carbon Dioxide Capture*. MIT Carbon Sequestration Forum X.

Downloaded from http://pubs.geoscienceworld.org/gsl/geoenergy/article-pdf/doi/10.1144/geoenergy2025-046/7859514/geoenergy2025-046.pdf by TU DelftLibrary user on 10 J

ISRM 1978. Suggested methods for determining tensile strength of rock materials. *International Journal of Rock Mechanics & Mining Sciences*, **15**, 99–103, http://dx.doi.org/10.1016/0148-9062(78)90003-7

Janjuhah, H.T. and Alansari, A. 2019. Offshore carbonate facies characterization and reservoir quality of Miocene rocks, Central Luconia, Offshore Sarawak, Malaysia. *Acta Geologica Sinica*, **94**, 1–20, https://doi.org/10.1111/1755-6724.13880

Janjuhah, H.T., Salim, A.M.A., Ghosh, D.P. and Wahid, A. 2017*a*. Diagenetic process and their effect on reservoir quality in Miocene carbonate reservoir, offshore Sarawak, Malaysia. In: *Icipeg 2016 Proceedings of the International Conference on Integrated Petroleum Engineering and Geosciences*. Springer, 545–548, https://doi.org/10.1007/978-981-10-3650-7

Janjuhah, H.T., Salim, A.M.A., Shah, M.M., Ghosh, D. and Alansari, A. 2017*b*. Quantitative interpretation of carbonate reservoir rock using wireline logs: a case study from Central Luconia, offshore Sarawak, Malaysia. *Carbonates Evaporites*, **32**, 591–607, https://doi.org/10.1007/s13146-017-0361-6

Josh, M., Esteban, L., Delle Piane, C., Sarout, J., Dewhurst, D.N. and Clennell, M.B. 2012. Laboratory characterisation of shale properties. *Journal of Petroleum Science and Engineering*, **88–89**, 107–124, https://doi.org/10.1016/j.petrol.2012.01.023

Kallu, R. and Roghanchi, P. 2015. Correlations between direct and indirect strength test methods. *International Journal of Mining Science and Technology*, **25**, 355–360, https://doi.org/10.1016/j.ijmst.2015.03.005

Kampman, N., Ellam, R.M., Bickle, M.J., Burnside, N.M., Shipton, Z.K., Chapman, H.J. and Nicholl, J.A. 2012. Pulses of carbon dioxide emissions from intracrustal faults following climatic warming. *Nature Geoscience*, **5**, 352–358, https://doi.org/10.1038/ngeo1451

Kaszuba, J.P., Navarre-Sitchler, A., Thyne, G., Chopping, C. and Meuzelaar, T. 2011. Supercritical carbon dioxide and sulfur in the Madison Limestone: a natural analog in southwest Wyoming for geologic carbon–sulfur co-sequestration. *Earth and Planetary Science Letters*, **309**, 131–140, https://doi.org/10.1016/j.epsl.2011.06.033

Krushin, J.T. 1997. Seal capacity of nonsmectite shale. *In:* Surdam, R.C. (ed.) *Seals, Traps, and the Petroleum System*. AAPG, 31–47.

Kuila, U., Dewhurst, D.N., Siggins, A.F. and Raven, M.D. 2011. Stress anisotropy and velocity anisotropy in low porosity shale. *Tectonophysics*, **503**, https://doi.org/10.1016/j.tecto.2010.09.023

Kuo, L.-C. 1997. Gas exsolution during fluid migration and its relation to overpressure and petroleum accumulation. *Marine and Petroleum Geology*, **14**, 221–229, https://doi.org/10.1016/S0264-8172(97)00003-2

Li, D. and Wong, L.N.Y. 2013. The Brazilian disc test for rock mechanics applications: review and new insights. *Rock Mechanics and Rock Engineering*, **46**, 269–287, https://doi.org/10.1007/s00603-012-0257-7

Liska, R.D. 1991. The history, age and significance of the *Globorotalia menardii* zone in Trinidad and Tobago, West Indies. *Micropaleontology*, **37**, 173–182, https://doi.org/10.2307/1485557

Liu, H.H., Zhang, G., Yi, Z.L. and Wang, Y. 2013. A permeability-change relationship in the dryout zone for CO_2 injection into saline aquifers. *International Journal of Greenhouse Gas Control*, **15**, https://doi.org/10.1016/j.ijggc.2013.01.034

Lunt, P. and Madon, M. 2017. A review of the Sarawak Cycles: history and modern application. *Bulletin of the Geological Society of Malaysia*, **63**, 77–101, https://doi.org/10.7186/bgsm63201704

Luquot, L. and Gouze, P. 2009. Experimental determination of porosity and permeability changes induced by injection of CO_2 into carbonate rocks. *Chemical Geology*, **265**, 148–159, https://doi.org/10.1016/j.chemgeo.2009.03.028

Madon, M. 1999. Chapter 12: Geological setting of Sarawak. *In: Petroleum Geology and Resources of Malaysia*. Petroliam Nasional Berhad (PETRONAS), 273–290.

Madon, M. and Redzuan, A.H. 1999. Tatau-Province. *In: The Petroleum Geology and Resources of Malaysia*. Petroliam Nasional Berhad (PETRONAS), 411–426.

Masoudi, R., Azran, M. *et al.* 2011. An integrated reservoir simulation-geomechanical study on feasibility of CO2 storage in M4 carbonate reservoir, Malaysia. Paper presented at the International Petroleum Technology Conference, November, Bangkok, Thailand, https://doi.org/10.2523/IPTC-15029-MSPTC 15029

McCloskey, S.M., Anderson, P.F. and Mirzaei, M. 2022. Reservoir characterization and comparison of seismicity-monitoring methods at West Seminole for CO_2 utilization and storage. *AAPG Bulletin*, **106**, 1899–1920, https://doi.org/10.1306/02252221037

Mellor, M. and Hawkes, I. 1971. Measurement of tensile strength by diametral compression of discs and annuli. *Engineering Geology*, **5**, 173–225, https://doi.org/10.1016/0013-7952(71)90001-9

Metcalfe, I. 2009. Late Palaeozoic and Mesozoic tectonic and palaeogeographical evolution of SE Asia. *Geological Society, London, Special Publications*, **315**, https://doi.org/10.1144/sp315.2

Metcalfe, I. 2011. Palaeozoic–Mesozoic history of SE Asia. *Geological Society, London, Special Publications*, **355**, https://doi.org/10.1144/sp355.2

Minaeian, V., Dewhurst, D.N. and Rasouli, V. 2017. Deformational behaviour of a clay-rich shale with variable water saturation under true triaxial stress conditions. *Geomechanics for Energy and the Environment*, **11**, 1–13, https://doi.org/10.1016/j.gete.2017.04.001

Moore, H.C. 1989. *Carbonate Diagenesis and Porosity*. Elsevier, https://doi.org/10.1016/0920-4105(92)90066-a

Morad, D., Nader, F.H. *et al.* 2018. Comparison of the diagenetic and reservoir quality evolution between the anticline crest and flank of an Upper Jurassic carbonate gas reservoir, Abu Dhabi, United Arab Emirates. *Sedimentary Geology*, **367**, 96–113, https://doi.org/10.1016/j.sedgeo.2018.02.008

Najibi, A.R., Ghafoori, M., Lashkaripour, G.R. and Asef, M.R. 2015. Empirical relations between strength and static and dynamic elastic properties of Asmari and Sarvak limestones, two main oil reservoirs in Iran. *Journal of Petroleum Science and Engineering*, **126**, 78–82, https://doi.org/10.1016/j.petrol.2014.12.010

Nazir, R., Momeni, E., Armaghani, D.J. and Amin, M.F.M. 2013. Correlation between unconfined compressive strength and indirect tensile strength of limestone rock samples. *Electronic Journal of Geotechnical Engineering*, **18**, 1737–1746, https://www.scopus.com/pages/publications/84882955701

Palchik, V. 2011. On the ratios between elastic modulus and uniaxial compressive strength of heterogeneous carbonate rocks. *Rock Mechanics and Rock Engineering*, **44**, 121–128, https://doi.org/10.1007/s00603-010-0112-7

Palchik, V. and Hatzor, Y.H. 2000. Correlation between mechanical strength and microstructural parameters of dolomites and limestones in the Judea Group, Israel. *Israel Journal of Earth Sciences*, **49**, 65–79, https://doi.org/10.1560/LGVQ-HA9E-P1X7-YRAT

Pereira Nunes, J.P., Seabra, G.S. and de Sousa, L.C. 2024. A review of CO_2-injection projects in the Brazilian Pre-Salt – storage capacity and geomechanical constraints. *International Journal of Greenhouse Gas Control*, **137**, 104232, https://doi.org/10.1016/j.ijggc.2024.104232

Perras, M.A. and Diederichs, M.S. 2014. A review of the tensile strength of rock: concepts and testing. *Geotechnical and Geological Engineering*, **32**, 525–546, https://doi.org/10.1007/s10706-014-9732-0

Pervukhina, M., Gurevich, B., Dewhurst, D.N., Golodoniuc, P. and Lebedev, M. 2015. Chapter 9: Rock physics analysis of shale reservoirs. *In:* Rezaee, R. (ed.) *Fundamentals of Gas Shale Reservoirs*. Wiley, 186–200.

Pierson, B., Ting, K.K., Pierson, B.J. and Ting, K.K. 2012. A review of porosity classification in carbonates: challenges in Miocene reservoirs of Central Luconia, offshore Sarawak. Paper presented at the International Conference on Integrated Petroleum Engineering and Geosciences (ICIPEG), Kuala Lumpur, Malaysia.

Pokrovsky, O.S., Golubev, S.V. and Schott, J. 2005. Dissolution kinetics of calcite, dolomite and magnesite at 25°C and 0 to 50 atm pCO_2. *Chemical Geology*, **217**, 239–255, https://doi.org/10.1016/j.chemgeo.2004.12.012

Profice, S., Lasseux, D., Jannot, Y., Jebara, N. and Hamon, G. 2012. Permeability, porosity and Klinkenberg coefficient determination on crushed porous media. *Petrophysics*, **53**, 430–438.

Rees, S. 2013. *Part One: Introduction to the Triaxial Testing*, GDS, www.gdsinstruments.com

Rehm, S.K. 2003. *The Miocene Carbonates in Time and Space On- and Offshore SW Palawan, Philippines*. Dissertation, Christian-Albrechts-Universität zu Kiel.

Riding, J.B. and Rochelle, C.A. 2009. Subsurface characterization and geological monitoring of the CO_2 injection operation at Weyburn, Saskatchewan, Canada. *Geological Society, London, Special Publications*, **313**, 227–256, https://doi.org/10.1144/SP313.14

Rimmelé, G. and Renard, F. 2010. Evolution of the petrophysical and mineralogical properties of two reservoir rocks under thermodynamic conditions relevant for CO_2 geological storage at 3 km depth. *Oil & Gas Science and Technology*, **65**, 565–580, https://doi.org/10.2516/ogst/2009071

Ringrose, P.S. 2018. The CCS hub in Norway: some insights from 22 years of saline aquifer storage. *Energy Procedia*, **146**, 166–172, https://doi.org/10.1016/j.egypro.2018.07.021

Sazali, W.M.L., Md Shah, S.S., Zuhaili Kashim, M., Kantaatmadja, B.P., Knuefing, L. and Young, B. 2019. The use of digital core analysis in understanding the effects of CO_2 aging to carbonates samples. Paper presented at the SPE Middle East Oil and Gas Show and Conference, March, Manama, Bahrain.

Sim, D. and Jaegar, G. 2006. Tectonostratigraphy and trap styles of the Half-Graben sub-province in West Luconia, offshore Sarawak. *Geological Society of Malaysia Bulletin*, **4**, 107–110, https://doi.org/10.7186/bgsm49200617

Siqueira, T.A., Iglesias, R.S. and Ketzer, J.M. 2017. Carbon dioxide injection in carbonate reservoirs – a review of CO_2-water-rock interaction studies. *Greenhouse Gases: Science and Technology*, **7**, 802–816, https://doi.org/10.1002/ghg.1693

Solomon, S. 2006. *Carbon Dioxide Storage: Geological Security and Environmental Issues–Case Study on the Sleipner Gas field in Norway*. Bellona Report, July.

Sterpenich, J., Sausse, J., Pironon, J., Géhin, A., Hubert, G., Perfetti, E. and Grgic, D. 2009. Experimental ageing of oolitic limestones under CO_2 storage conditions. Petrographical and chemical evidence. *Chemical Geology*, **265**, 99–112, https://doi.org/10.1016/j.chemgeo.2009.04.011

Tjia, H.D. 2000. Tectonic and structural development of Cenozoic basins of Malaysia. Paper presented at the Geological Society of Malaysia Annual Conference, 8–9 September, Pulau Pinang, Malaysia.

Tjia, H.D. 2012. The Paleo-orientations of Northwestern Borneo and adjacent South China sea basins. *Indonesian Journal on Geoscience*, **7**, 67–76, https://doi.org/10.17014/ijog.7.2.67-76

Vialle, S. and Vanorio, T. 2011. Laboratory measurements of elastic properties of carbonate rocks during injection of reactive CO_2-saturated water. *Geophysical Research Letters*, **38**, 1–5, https://doi.org/10.1029/2010GL045606

Downloaded from http://pubs.geoscienceworld.org/gsl/geoenergy/article-pdf/doi/10.1144/geoenergy2025-046/7859514/geoenergy2025-046.pdf by TU DelftLibrary user on 10 J

Wade, B.S., Pearson, P.N., Olsson, R.K., Fraass, A.J., Leckie, R.M. and Hemleben, C. 2018. Taxonomy, biostratigraphy, and phylogeny of Oligocene and lower Miocene *Dentoglobigerina* and *Globoquadrina*. *In: Atlas of Oligocene Planktonic Foraminifera*. Cushman Foundation for Foraminiferal Research Special Publication, **46**, 331–384.

Warrlich, G.M.D., Adams, E.W., Ryba, A., Tam, T., Ting, K.K. and Tang, H.K. 2019. What matters for flow and recovery in carbonate gas reservoirs: insights from the mature Central Luconia Province, offshore Sarawak, Malaysia. *American Association of Petroleum Geologists Bulletin*, **103**, 691–721, https://doi.org/10.1306/09051817219

Wayne, M.A. 2008. *Geology of Carbonate Reservoirs: The Identification, Description, and Characterization of Hydrocarbon Reservoirs in Carbonate Rocks*. Wiley.

Widyanita, A.W. 2017. The importance of integrated screening and assessments for future potential CO_2 storage sites identification. In: *79th EAGE Conference and Exhibition 2017*. European Association of Geoscientists & Engineers, https://doi.org/10.3997/2214-4609.201701320

Wilson, M.E.J., Ee Wah, E.C., Dorobek, S. and Lunt, P. 2013. Onshore to offshore trends in carbonate sequence development, diagenesis and reservoir quality across a land-attached shelf in SE Asia. *Marine and Petroleum Geology*, **45**, 349–376, https://doi.org/10.1016/j.marpetgeo.2013.03.011

Xiao, Y., Macleod, G., Advocate, D.M., Reaves, C. and Pottorf, R.J. 2011. Natural CO_2 occurrence in geological formations and the implications on CO_2 storage capacity and site selection. *Energy Procedia*, **4**, 4688–4695, https://doi.org/10.1016/j.egypro.2011.02.430

Yang, Y. and Aplin, A.C. 2007. Permeability and petrophysical properties of 30 natural mudstones. *Journal of Geophysical Research*, **112**, B03206, https://doi.org/10.1029/2005JB004243

Zaidin, M.F., Priyatna Kantaatmadja, B., Chapoy, A., Ahmadi, P. and Burgass, R. 2019. Experimental study to estimate CO_2 solubility in a high pressure high temperature HPHT reservoir carbonate aquifer. Paper presented at the SPE Middle East Oil and Gas Show and Conference, March, Manama, Bahrain, https://doi.org/10.2118/195003-ms

Zambrano, M., Tondi, E., Mancini, L., Arzilli, F., Lanzafame, G., Materazzi, M. and Torrieri, S. 2017. 3D pore-network quantitative analysis in deformed carbonate grainstones. *Marine and Petroleum Geology*, **82**, 251–264, https://doi.org/10.1016/j.marpetgeo.2017.02.001

Zampetti, V., Schlager, W. and Konijnenburg, J.V.A.N. 2003. Depositional history and origin of porosity in a Miocene carbonate platform of Central Luconia, offshore Sarawak. *Bulletin of the Geological Society of Malaysia*, **47**, 139–152, https://doi.org/10.7186/bgsm47200311

Zhang, R. and Wu, Y.-S. 2018. Hydrologic, mechanical, thermal, and chemical process coupling triggered by the injection of CO_2. *In:* Newell, P. and Ilgen, A.G. (eds) *Science of Carbon Storage in Deep Saline Formations*. Elsevier, 361–381, https://doi.org/10.1016/b978-0-12-812752-0.00016-2

Zheng, H., Feng, X.T. and Pan, P.Z. 2015. Experimental investigation of sandstone properties under CO_2-NaCl solution-rock interactions. *International Journal of Greenhouse Gas Control*, **37**, 451–470, https://doi.org/10.1016/j.ijggc.2015.04.005

Zhou, X., Zeng, Z., Liu, H. and Boock, A. 2009. Laboratory testing on geomechanical properties of carbonate rocks for CO_2 sequestration. Paper presented at the 43rd U.S. Rock Mechanics Symposium and 4th U.S.-Canada Rock Mechanics Symposium, June, Ashville, NC.

Zin, I.C.M. 1997. Tectonics evolution and sedimentation history of the Sarawak Basin. *Geological Society of Malaysia, Bulletin*, **41**, 41–52, https://doi.org/10.7186/bgsm41199705

Downloaded from http://pubs.geoscienceworld.org/gsl/geoenergy/article-pdf/doi/10.1144/geoenergy2025-046/7859514/geoenergy2025-046.pdf by TU DelftLibrary user on 10 J